Nano-Composite Dielectrics on Medium-Voltage Model Cables

1013885

Nano-Composite Dielectrics on Medium-Voltage Model Cables

1013885

Technical Update, December 2007

EPRI Project Manager
M. Olearczyk

DISCLAIMER OF WARRANTIES AND LIMITATION OF LIABILITIES

THIS DOCUMENT WAS PREPARED BY THE ORGANIZATION(S) NAMED BELOW AS AN ACCOUNT OF WORK SPONSORED OR COSPONSORED BY THE ELECTRIC POWER RESEARCH INSTITUTE, INC. (EPRI). NEITHER EPRI, ANY MEMBER OF EPRI, ANY COSPONSOR, THE ORGANIZATION(S) BELOW, NOR ANY PERSON ACTING ON BEHALF OF ANY OF THEM:

(A) MAKES ANY WARRANTY OR REPRESENTATION WHATSOEVER, EXPRESS OR IMPLIED, (I) WITH RESPECT TO THE USE OF ANY INFORMATION, APPARATUS, METHOD, PROCESS, OR SIMILAR ITEM DISCLOSED IN THIS DOCUMENT, INCLUDING MERCHANTABILITY AND FITNESS FOR A PARTICULAR PURPOSE, OR (II) THAT SUCH USE DOES NOT INFRINGE ON OR INTERFERE WITH PRIVATELY OWNED RIGHTS, INCLUDING ANY PARTY'S INTELLECTUAL PROPERTY, OR (III) THAT THIS DOCUMENT IS SUITABLE TO ANY PARTICULAR USER'S CIRCUMSTANCE; OR

(B) ASSUMES RESPONSIBILITY FOR ANY DAMAGES OR OTHER LIABILITY WHATSOEVER (INCLUDING ANY CONSEQUENTIAL DAMAGES, EVEN IF EPRI OR ANY EPRI REPRESENTATIVE HAS BEEN ADVISED OF THE POSSIBILITY OF SUCH DAMAGES) RESULTING FROM YOUR SELECTION OR USE OF THIS DOCUMENT OR ANY INFORMATION, APPARATUS, METHOD, PROCESS, OR SIMILAR ITEM DISCLOSED IN THIS DOCUMENT.

ORGANIZATION(S) THAT PREPARED THIS DOCUMENT

Rensselaer Polytechnic Institute

NOTE

For further information about EPRI, call the EPRI Customer Assistance Center at 800.313.3774 or e-mail askepri@epri.com.

CITATIONS

This report was prepared by

Rensselaer Polytechnic Institute
110 8th Street
Troy, NY 12180-3590

Principal Investigators
J.K. Nelson
L.S. Schadler
R. Smith
L.Hui

This publication is a corporate document that should be cited in the literature in the following manner:

Nano-Composite Dielectrics on Medium-Voltage Model Cables. EPRI, Palo Alto, CA: 2007. 1013790.

PRODUCT DESCRIPTION

EPRI early recognized the potential for nanotechnology in power distribution and started a program in 2003 to explore the possibilities of using the technology to enhance the properties of high-voltage (HV) cable dielectrics based on both polyethylene and on ethylene-propylene rubber. This research resulted in encouraging findings, particularly for a formulation based on functionalized silicon dioxide nanoparticles in a cross-linked polyethylene (XLPE) polymer. Following this success, EPRI entered into a joint agreement with Dow Chemical to take the technology commercial, an effort that has involved Rensselaer in tasks associated with switching the base resin and refining some of the processing parameters. This interim report chronicles this ongoing effort to develop nanodielectrics for HV utility cable applications.

Results and Findings

To date, the materials developed in this program have only been produced in small quantities using melt-mixing techniques. Although properties such as viscosity have been measured to insure that extrusion will still be possible, extension to the commercial scale will involve additional effort since it is not certain that all parameters developed for molded samples will be appropriate to industrial-scale production. Consequently, a major part of Rensselaer's ongoing work is devoted to supporting the scale-up activity at Dow Chemical and to technology transfer activities. Preliminary work in this category is devoted to processing and dielectric strength testing to obtain a common measure to apply at both Dow Chemical and Rensselaer. Since the quality of the formulation depends on dispersion, field emission scanning electron microscopy plays a major role in material assessment. Furthermore, a quantitative measure of dispersion has been found necessary.

While microscopy and breakdown strength may be appropriate as quality control measures to optimize polymer processing, such metrics are not very effective in mechanistic research. To improve mechanistic analyses, a number of other techniques are being used that can provide information on such factors as charge trapping, internal electric fields, "hot" electron scattering, and carrier mobility. An improved metric for mechanistic analysis can provide an informed basis for the engineering of nanodielectrics for a variety of purposes. To place the mechanistic studies in proper context, the report summarizes the state of knowledge on nanocomposites and suggests the most likely mechanisms that account for their unique properties.

Challenges and Objectives

Control of particle interface is key to tailoring nanodielectric properties. Identified in an earlier study, chemical functionalization is one way control can be exercised. However, the underlying mechanisms must be understood and the role of the interface in controlling charge transport and storage requires further investigation.

Applications, Value, and Use

This ongoing project involves work in support of scale-up efforts to commercialize the technology for the cable industry. This work is being supplemented by more fundamental research aimed at understanding charge transport and storage, which permits engineering of nanodielectrics in an informed way.

EPRI Perspective

The technology transfer aspects of the program at both Rensselaer and Dow Chemical have focused on using alternating current (ac) dielectric strength to measure the efficacy of the technology. Although tests at Rensselaer continue to show improvements in dielectric strength up to a loading of 12 ½%, this is not always seen in tests at Dow Chemical. Though the reason for this discrepancy is not specifically known, it may result from poor dispersion, the quality of dispersion a key factor in nanocomposite performance. Quantifying dispersion is currently a manual and very time-consuming process. As work proceeds, use of recognition software to automate the process is planned. Also, use of advanced methods such as electroluminescence and pulsed electroacoustic analysis that account for differences produced through particle size, loading, and surface chemistry will provide further insight into the operation of internal interfaces.

Approach

This is an interim report of ongoing work. The tasks described have been undertaken in tandem and, thus, many have not yet been completed.

Keywords

Cable
Medium-voltage cable
Nanodielectric composite

ABSTRACT

This report chronicles ongoing effort to develop nanodielectrics for HV utility cable applications. Two primary thrusts are described. The first involves work in support of scale-up efforts in order to try to commercialize the technology to provide benefits for the cable industry. This is supplemented by more fundamental research aimed at the understanding of charge transport and storage in these new materials to permit the engineering of nanodielectrics in an informed way.

ACKNOWLEDGMENTS

CONTENTS

xii

LIST OF FIGURES

LIST OF TABLES

1
BACKGROUND AND INTRODUCTION

In the context of this report, nanodielectrics are defined as the incorporation of nanoparticles into a polymer matrix to form a nanocomposite, and a nanoparticle is usually defined as having at least one dimension less than 100 nm (although most un agglomerated particulates today are usually about 20 nm or less. Following an initial paper by Nelson et al. [1] using amorphous epoxy resin as a base material, the whole area of nanocomposites has attracted unprecedented interest by the dielectrics community in the last 5 years. This burgeoning effort has resulted in a special issue of the IEEE Transactions of Dielectrics and Electrical Insulation edited by Dissado and Fothergill [2] and a second dedicated issue edited by Nelson and Schadler will appear in 2008. An indication of the interest shown can also be measured by the papers submitted to technical conferences and the special sessions organized to accommodate them.

EPRI recognized the potential for this technology and started a program in 2003 to explore the possibilities for using this technology for enhancing the properties of HV cable dielectrics based on both polyethylene and on ethylene-propylene rubber. This culminated in encouraging findings (particularly for a formulation based on functionalized silicon dioxide nanoparticles incorporated in a cross-linked polyethylene (XLPE) polymer [3,4]. Following this, EPRI entered into a joint agreement with Dow Chemical to take this technology to the commercial scale which involved Rensselaer in the tasks associated with switching the base resin and refining some of the processing parameters. This effort was documented [5] in March 2007 and characteristics of the nanocomposites based on a Dow Chemical resin were chronicled and compared with the previous studies conducted on a competitor's material. However, changes were not made in the nanophase filler or in its functionalization since it had already been optimized in the prior study. The 2007 report outlines the development of this initiative and provides an overview of the basic principles involved. As a result, these aspects will not be repeated here.

1.1 The Ongoing Development

The effectiveness of these materials is intimately tied to the processing steps and parameters used in the compounding and formulation. This is, in part, because of the inherent tendency of particles of this size to agglomerate. In particular, it is well known that the electric strength of most polymers decreases upon adding conventional (micron scale) filler materials. Consequently, any agglomeration resulting in clusters greater than about 100nm can be expected to severely erode any benefits obtained from this technology. It is for this reason that a significant level of effort has been expended over the last 3 years to optimize the pre-processing, compounding, cross-linking, molding and post-processing. Getting all these steps correct is critical to the formulation of a successful nanodielectric.

1.1.1 Scale-up activities

To date, these materials have only been produced in small quantities using melt-mixing techniques [3-4]. Although properties such as viscosity have been measured to insure that extrusion will still be possible, the extension to the commercial scale will clearly involve some additional effort since it is by no means certain that all of the parameters developed for molded samples will be appropriate to the industrial scale production. For this reason a major part of the ongoing work at Rensselaer is devoted to the support of the scale-up activity at Dow Chemical and to technology transfer activities. Preliminary work in this category is described in Chapters 2 and 3 devoted to the processing and to dielectric strength testing in order to try to obtain a common measure to apply at both institutions (Dow Chemical and Rensselaer). Since it is known that the quality of the formulation is intimately dependent on the dispersion, the use of field emission scanning electron microscopy plays a major role in the assessment of these materials. Furthermore, as part of this work a quantitative measure of the dispersion has been found necessary. Initial research on this aspect has been provided in Chapter 4.

1.1.2 Tailoring properties

Later in this report, some mechanistic insight is provided on the basis of this, and other, work. However, as a preliminary view, Figure 1-1 shows an idealized situation in which (spherical) particles are depicted in a polymer matrix. Figure 1-1 (a) illustrates the situation for a microparticle which is surrounded by an "interaction zone" having a radial dimension (here exaggerated) of about 10 nm. In the case of fillers of microscopic dimensions, the interaction zone is insignificant in extent. This contrasts, however, with the situation depicted in Figure 1-1 (b) where, for the same weight loading, numerous nanoparticles exhibit not only a much increased surface area, but are also characterized by interactions between the interfering interaction zones. Indeed, although the material may have been formulated from a filler phase and a base resin, the resultant material is dominated by the interaction zones. In this sense, philosophically speaking, if the nanoparticles become small enough, it really constitutes an entirely new material. It is therefore to be expected that the properties of nanodielectrics will, to a large extent, be controlled by the interaction zones formed at the particle interfaces.

Viewed in this way, it may be seen that the control of the particle interface is the key to tailoring the properties of nanodielectrics. The use of chemical functionalization is one way in which this control can be exercised, and this has been highlighted in an earlier report [3]. However, in order to do this, the underlying mechanisms must be understood and the role of the interface in controlling the charge transport and storage in this new class of material needs to be isolated. While the use of microscopy and breakdown strength may be appropriate as quality control measures to optimize polymer processing, such metrics are not very effective in mechanistic research. In order to do this, advantage is being taken of a plurality of other techniques which can provide information on charge trapping, internal electric fields, "hot" electron scattering, carrier mobility, etc. Chapter 5 provides some, again very preliminary, results in this area in order to obtain an informed basis for the engineering of nanodielectrics for a variety of purposes.
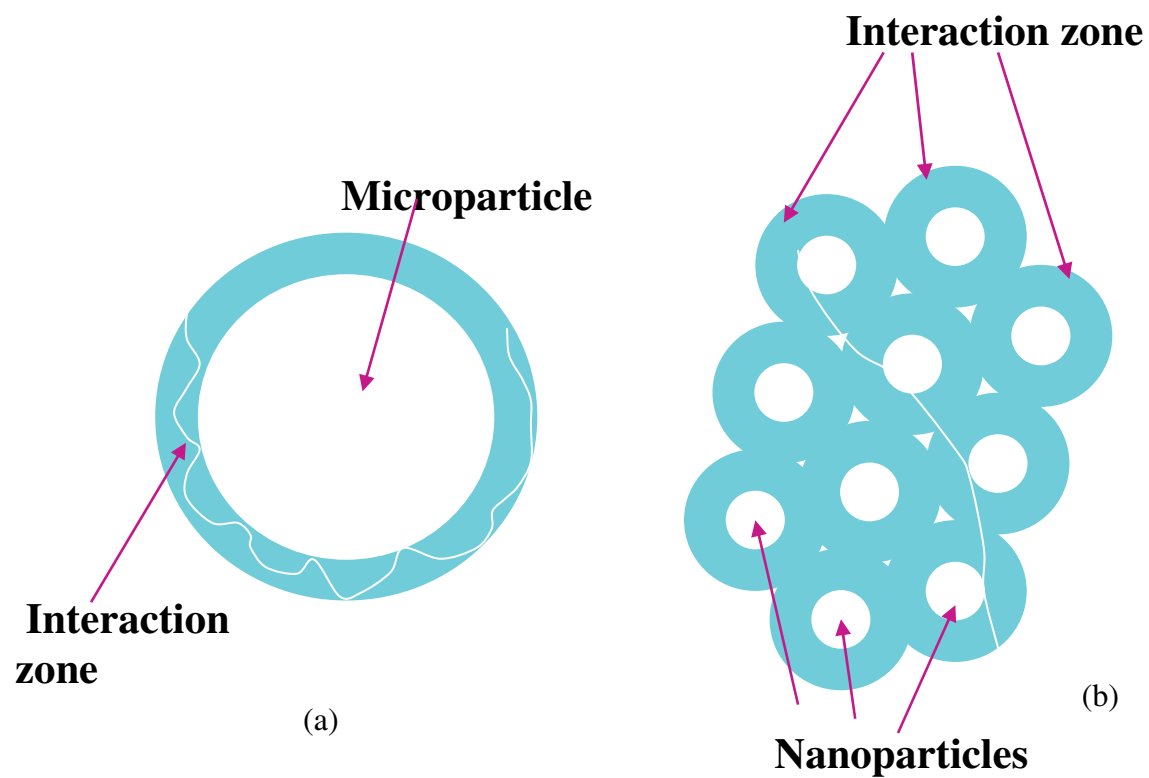
Figure 1-1
Schematic representation of (a) a microparticle, and (b) an assembly of nanoparticles. (*Not to scale*).

2

PROCESSING DEVELOPMENT AND TECHNOLOGY TRANSFER

2.1 Material Processing and Measurement Refinements

Since the April 2007 report to EPRI [5], the production of samples has been improved and an additional measurement technique has been adopted. Specifically, the following changes in procedure have been made:

- After discussion of mixing protocols with Dow Chemical in September, 2007, RPI has adopted the practice of adding the dicumyl peroxide crosslinking agent to LDPE in the melt mixer after first reducing the melt temperature and mixing speed. The procedural changes are provided in Table 2-1.

Table 2-1
Changes in the Introduction of Crosslinking Dicumyl Peroxide (DCP)

	Protocol	
	Previous ("Hot" Method)	New Sept. 2007 ("Cold" Method)
Weight Percent DCP	2.0	2.0
Begin Material Cooldown	N/A	6 minutes after mixing begins
Melt Temp. at DCP Addition	~150°C	~125°C
Mixer Speed Before (After) DCP Addition	60 (60) rpm	60 (20) rpm
DCP Added	6 minutes after mixing begins	~15 minutes after mixing begins (depends on LDPE cooling time)
Total LDPE Mixing Time	10 minutes	~19 minutes

The change may be summarized as follows: whereas previously, liquefied DCP was added to the hot melt (melt temperature of approximately 150°C), the new procedure calls for the addition of the liquefied DCP at 125-130°C. To facilitate this temperature change, the temperature heating setpoint is lowered to 120°C, and the mixing speed lowered to 20 rpm to help prevent a subsequent rise in temperature over approximately 135°C. This change was incorporated due to discussions with Dow regarding the reaction characteristics of DCP/LDPE at elevated temperatures, possibly resulting in premature crosslinking, as well as personnel safety when working with heated peroxides generally.

A comparison of 60 Hz breakdown strength between materials prepared by the "hot" and "cold" method is given in Section 3 of this report.

- A study of the extent to which the polyethylene is properly crosslinked has been undertaken. ASTM Standard D 2765-01 "Test Methods for Determination of Gel Content and Swell Ratio of Crosslinked Ethylene Plastics" gives a procedure using a prescribed solvent (xylenes) to determine the relative level to which a material is crosslinked. Crosslinking consistency should be maintained so that observed improvements in, for example, breakdown strength of one type of material over another, are not actually a reflection of the increased viscosity due to higher crosslinking. It was determined, presumably due to the volatility of the dicumyl peroxide mixed into the materials, that the time between the melt-mixing of material and its molding in the hot press (where the bulk of crosslinking is intended to take place), was crucial in producing materials with the highest level of crosslinking possible. Tests were conducted on materials that had been melt-mixed and pressed on the same day, as well as those melt-mixed and then pressed two days later. Note that this testing was done before the distinction between the "hot" and "cold" mixing methods was made; thus this was done on "hot" method material.

  The standard calls for the determination of a swell ratio (SR), calculated as follows:

  $$SR = 1 + K(W_g - W_d)/(W_o - W_e) \qquad\qquad \text{Eq. 2-1}$$

  where K=1.07 for polyethylene, W_g = weight of xylene-swolen gel, W_d = weight of the gel after vacuum drying, W_o = original polymer weight (not including filler), and W_e = weight of the removed polymer and filler. Thus the higher the swell ratio, the more the material was affected by the xylene solvent, and the lower the relative amount of crosslinking. The standard does not provide for the calculation of an absolute amount of percent crosslinking, but does allow for comparison between materials, as given in Table 2-2.

  The data indicate that there is indeed a reduction in crosslinking when the time between melt-mixing and hot pressing is not kept to a minimum. In fact, early tests on XLPE that was mixed and then pressed two weeks later, showed near total dissolution of the polyethylene by the xylene solvent, indicating that essentially no crosslinking had taken place.

As a result of the swell ratio testing, it is now standard procedure to mix materials and press samples the same day.

Table 2-2
Tested Swell Ratios for Same Day Mixing/Pressing and Two Days Between

Material	Same Day	Two Days
XLPE	2.58	5.18
12-1/2% Microcomposite	3.22	4.71
12-1/2% Untr. Nanocomposite	4.04	5.58
12-1/2% VS-Nanocomposite	3.49	5.27

- The calculation of breakdown strength using pressed samples of multiple recesses requires accurate measurement of each recess thickness. Figure 2-1 provides a simple sketch of this procedure, with the improvement.
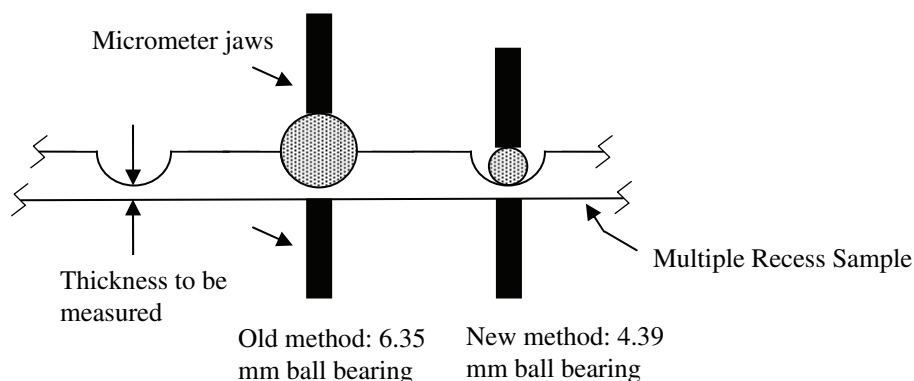
Figure 2-1
Sketch of the old and new method for measuring recess thickness for breakdown samples

It was found that sometimes, since pliable Teflon ball bearings are used to create the recesses in the samples (to prevent potential mold damage from steel contacting steel), the resulting recesses are sometimes enough out-of-round such that the 6.35 mm (¼") steel ball bearings used for measurement do not make complete contact with the bottom of the recess. This contact is of course necessary for accurate recess thickness measurement. The problem was evidenced by the lack of high repeatability of the measurement, and was accounted for by taking the average of three measurements as the value used in calculations of applied breakdown field intensity. Use of a smaller bearing allows for a much higher repeatability, within 5 μm (2/10,000"), since the smaller

bearing automatically seeks the bottom (and thus, the thinnest part) of the recess. This simple fix to the problem has provided a higher degree of confidence in breakdown results.

2.2 Microscopy

As part of the ongoing quality assurance, electron microscopy using a field emission scanning electron microscope (FESEM) is used to ensure good dispersion of the nanoparticles in the composite materials. In that regard, Section 4 of this report presents a new quantification procedure which will be used to describe the dispersion (the degree to which macroscopic particles are reduced to their primary particle size), and the distribution (the degree to which the particles and agglomerates are evenly spread throughout the mixture). However, in the interest of completeness, micrographs are here presented to illustrate, qualitatively, the progress made recently (especially in light of the change from the "hot" to "cold" mixing methods).
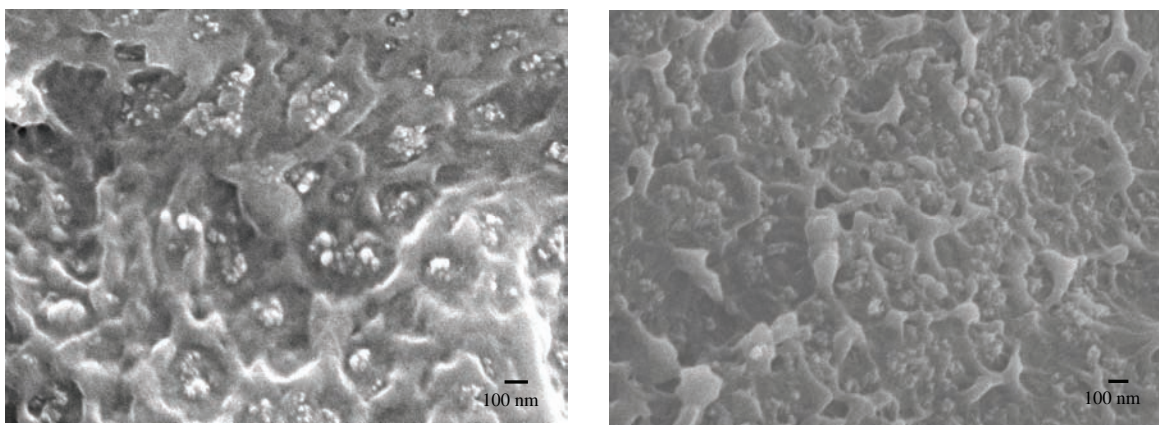
Figure 2-2
Micrographs of 12-1/2% Nanocomposite Mixed via the "Hot" Method
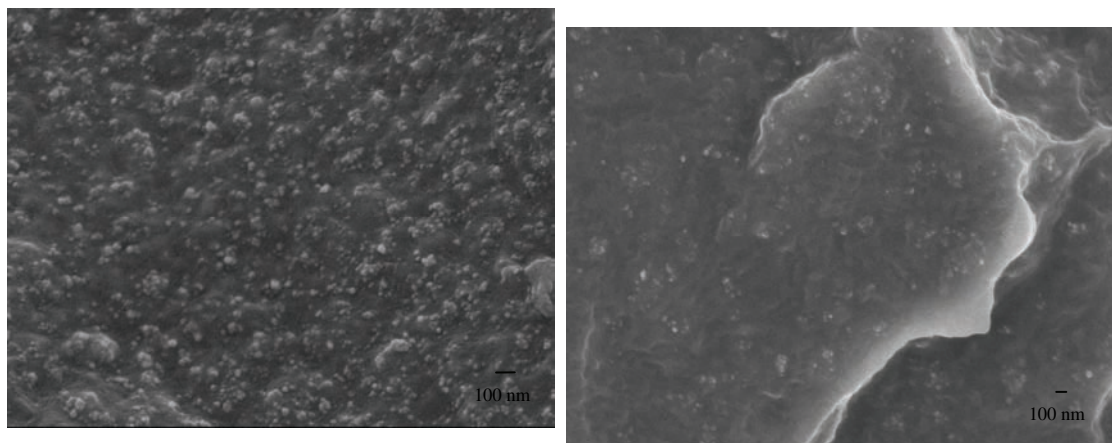
Figure 2-3
Micrographs of 12-1/2% Nanocomposite Mixed via the "Cold" Method

The micrographs seem to indicate that the addition of the peroxide at a reduced temperature has the added benefit of providing better distribution of particles with smaller agglomerates. This is presumably due to the increase in viscosity which accompanies the lower melt temperature, and thus the increased mixing shear at the rotor / melt interface.

2.3 Dow/RPI Technology Transfer

A working meeting between Dow, EPRI, and RPI was held on September 13th and 14th, 2007 at Dow Chemical in New Jersey. Discussed, amongst other things, was consistency of processing and testing procedures between RPI and Dow, so that meaningful comparisons might be made between test results on material processed and tested at Dow from that done at RPI. The following processing facts came to light during the meeting:

- RPI has been using a pre-melt dry mix of LDPE pellets and nanoparticles in a high-speed dual asymmetric centrifuge (DAC). It is believed that pre-coating polymer pellets in this way increases the ultimate particle dispersion; further that the mechanical agitation of the nanoparticles by the (much larger) pellets helps to break up macroscopic particle agglomerations. Dow's method does not include this step.

- Dow's addition of peroxide and that of RPI were different (the details of this difference are presented in Section 2.1). After discussion of the matter, RPI has decided to follow the Dow procedure (the "cold" method of mixing) from now on.

- Dow had been using, previous to the meeting, mixer rotors (of the Banbury type) which did not provide the highest shear possible, according to the manufacturer. Subsequent to the meeting, Dow has agreed to change to the high-shear (Roller type) rotors, similar to those used at RPI (Figure 2-4).

- Dow's pressed samples for breakdown testing are laminar, with evaporated contacts located in several spots on the pressing, rather than the multiple-recess type of pressing that RPI uses. No inconsistency in breakdown results is expected due to this different sample type, however, and therefore change by neither Dow nor RPI is planned. However, in comparing breakdown results between the two laboratories, account must be taken of size effects. This has been discussed [4] in relation to the gap size used, but it is also well known that an area effect exists which depresses the electric strength for larger test areas.

Figure 2-4
Roller Type High Shear Rotors Used by Both RPI and Dow

3
NANOCOMPOSITE ELECTRIC STRENGTH STUDIES

3.1 Comparison of Loading Optimization

In the spring of 2006, the polyethylene supplier was changed from Borealis to Dow. The Borealis material contained crosslinking DCP while the Dow material did not. In any case, the original 60 Hz breakdown optimization of vinylsilane-treated nanocomposites using the Borealis material had revealed a local maximum at or near 12½ wt%. Since the April 2007 EPRI report was submitted, a re-optimization of 60 Hz breakdown strength, from tests using Dow material, has been conducted. Table 3-1 presents the Weibull size (η) and shape (β) parameters for the Dow testing. As an important aside, it should be remembered that RPI's practice is to report AC data in the form of peak kV/mm (rather than V/mil), and that only points from the relatively horizontal portion of the breakdown field vs. thickness plot are included. For this work, the thickness range for the reported data is 0.1-0.3 mm. Failure to do this will cause inflated breakdown results which are not representative of those to be expected in bulk dielectrics.

Table 3-1
Weibull Size (η) and Shape (β) Parameters for the Dow Base XLPE and VS-Treated Nanocomposites (weight percents given)

	XLPE	**5%**	**7½%**	**10%**	**12½%**	**15%**
η (peak kV/mm)	182.3	211.7	205.5	214.6	247.2	214.0
β	2.79	4.03	2.36	3.11	2.36	3.39

Figure 3-1 illustrates a comparison between the Borealis and Dow optimizations. Interestingly, the two material supplies affected the test results in varying amounts, except at the 12½ wt% loading, where the Dow polyethylene not only displayed another 60 Hz breakdown maximum, but the value of the Weibull characteristic breakdown field intensity η was nearly identical to that of the Borealis. This is further evidence that the incorporation of the filler produces a material whose properties (or at least 60 Hz breakdown strength) seem to be more dependent on the filler amount than on the properties of the host polymer and filler themselves.
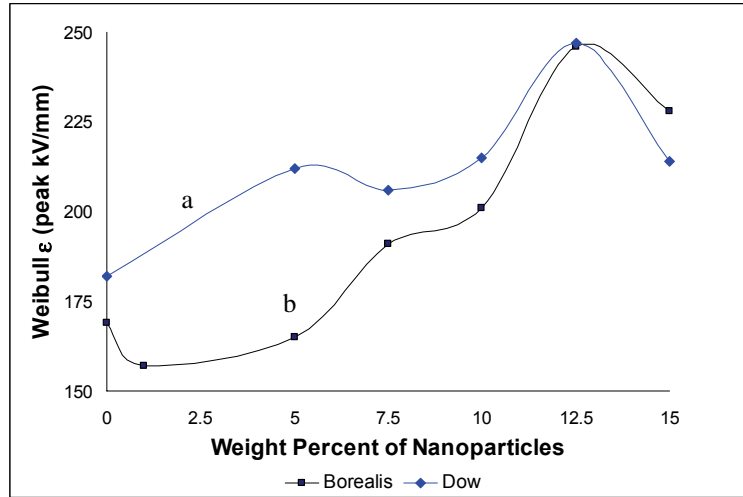
Figure 3-1
Comparison of Dow (a) and Borealis (b) Hz Breakdown Strengths for Optimization

3.2 Comparison of "Hot" and "Cold" Mixing Methods

The Dow data presented in Section 3.1 (curve (a) of Figure 3-1) actually consists of data from material mixed under both the "hot" and "cold" mixing methods (see Table 2-1 for an explanation of the two methods). In Figure 3-2 these same data points are separated with respect to the two methods to help understand their influence upon 60 Hz AC breakdown.
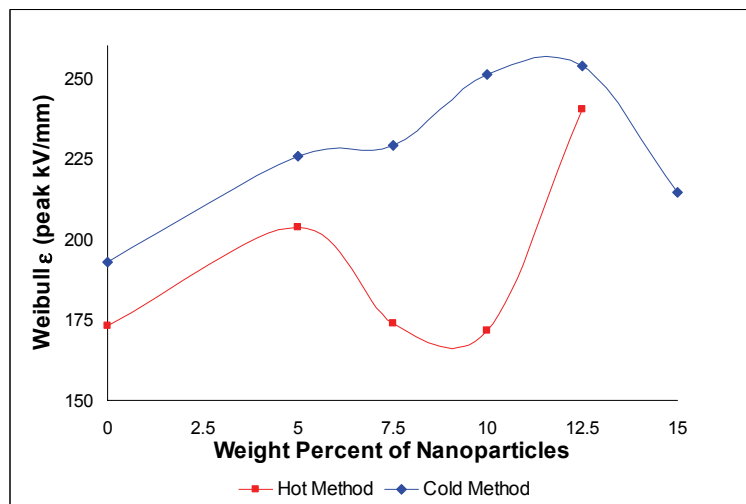
Figure 3-2
60 Hz Breakdown Strength - Hot (a) vs Cold (b) Mixing Methods for 12-1/2% VS-Nanocomposites (Dow Polyethylene). This represents the same data as curve (a) of Figure 3-1.

It is clearly seen that the cold method creates a material that outperforms that made by the hot method. Ostensibly, the dicumyl peroxide crosslinking agent is less degraded when it goes into the hot press for materials mixed under the cold method conditions.

3.3 Composites Mixed at Dow and Pressed and Tested at RPI

During the September 13th-14th meeting at Dow, material was mixed using two different methods. In the first method, polymer and vinylsilane-nanoparticles were pre-mixed at room temperature in a (low speed) horizontal axis dry mixer, then were blended in a melt mixer with high-shear rotors at 60 rpm. After cooling the mix down to ~125°C and reducing the mixing speed to 20 rpm, DCP was added. The resulting material was split roughly in half, for RPI to press and AC breakdown test one half while Dow would do the same using the other half. Another batch was produced and split in half as before, but this time there was no pre-blend. The purpose of this mixing and splitting of batches was that Dow and RPI would each independently test the materials to determine if there exist significant differences in testing between the two facilities. While the original intent was that all hot pressing would take place at Dow, the pneumatic supply for the Dow presses was unavailable that day; thus the Dow-produced, RPI-tested material was pressed at RPI.

Table 3-2
Weibull Size (η) and Shape (β) Parameters for 12-1/2% VS-Nanocomposite mixed at Dow, pressed and tested at RPI.

	With Pre-Blend	Without
η (peak kV/mm)	220.2	212.2
β	5.37	4.71

Table 3-2 presents the results for the Dow-mixed material that was pressed and tested at RPI. While it does appear that a difference exists between the pre-blended and non pre-blended material, the size of each data set is not very large. Because of the low speed of the Dow dry mixer, it is doubtful that this is a contributing factor.

To provide a comparison between the materials mixed, pressed, and tested at Dow from those mixed at Dow but pressed and tested at RPI, Figure 3-3 is presented below. Since there was essentially no difference between the results for the RPI-tested materials with or without the dry pre-blend (Table 3-2), all the RPI-tested data points have been combined into one data set on the graph. The cluster of data points at the left-hand end of the figure are the breakdown results (for thicknesses between 0.1 and 0.3 mm) for the RPI-tested material. Fitting a power law trend line to that data, and continuing the trend line to include a thickness of 1.0 mm, shows that the RPI-pressed and tested material outperformed the Dow-pressed and tested material. However, it must be remembered that the sample thickness effect illustrated by the shape of the trend line in the figure is only part of a broader <u>volume</u> effect which exists in the breakdown of solid dielectrics [6]. The Dow-produced samples are tested using two 12.7 mm (½") radius spherical electrodes, while the RPI test consists of one 3.2 mm (1/8") radius electrode. Thus, the RPI-pressed samples utilize a smaller surface area than the Dow-pressed samples, likely contributing to the apparent improvement in results of RPI over Dow.

60 Hz Breakdown of Materials Mixed at Dow
Mixed on 9/14/07 at the Weston Canal Center, NJ
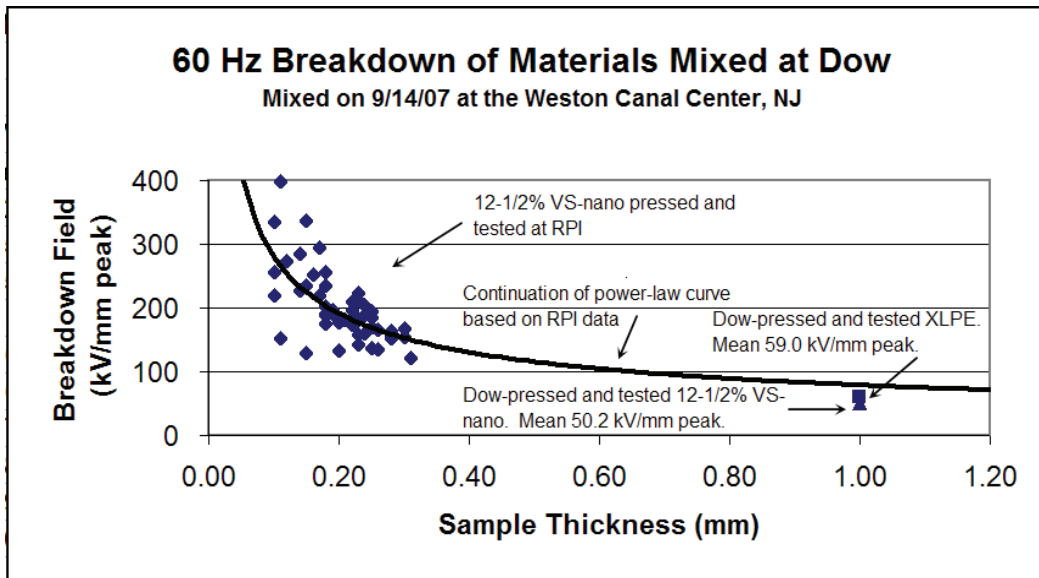
Figure 3-3
Comparison of AC breakdown results for Dow-mixed nanocomposites.

While direct comparison between the Dow and RPI pressing and testing methods is important, Figure 3-3 also illustrates that the Dow data do not show a breakdown improvement of the nanocomposite over the base XLPE. This is further depicted later in Figure 7-1. RPI testing has demonstrated the contrary: RPI <u>did</u> see an improvement of the Dow-mixed nanocomposite over the RPI-mixed base XLPE ($\eta = 182$ for the RPI base XLPE versus ~215 for the Dow-mixed nanocomposite).

4
QUANTIFICATION OF MIXING

The degree of mixing in composites is an important aspect in determining material quality. For nanofillers, because of their high surface-volume ratio, the nanoparticles tend to agglomerate; this will decrease the interface region between nano particles and the polymer matrix, which is known to play a vital role in nanocomposite behavior [7,8] . A uniform mixing is always sought, but the judgment of the mixing made by the naked eye is generally subjective and the results can vary from person to person. The meaning of quantification of mixing is to provide an objective judgment of the studied nanocomposites, and to facilitate comparison of the degree of mixing between nanocomposites with different loadings, different fillers, different processing strategies and the like.

In this chapter, several analysis methods employed in spatial point pattern statistics are applied to nanocomposites, and a novel method to quantify the degree of mixing by dispersion and distribution respectively is proposed.

4.1. Introduction to composite quantification

4.1.1. *Statistical analysis of microstructure*

Statistical analysis can be used to quantify the microstructure of materials. To carry out a statistical analysis of microstructure, there are several well defined steps [9]:

(1) Take an appropriate micrograph of the target materials. Depending on the scale and characteristics of materials, optical graph, scanning electron micrograph (SEM) or transmission electron micrograph (TEM) are frequently used to acquire the image of materials' microstructure.

(2) Choose a proper sampling. It is expected that the small regions chosen to be analyzed can represent fully the whole population.

(3) Digital image processing methods are sometimes used to process the micrograph, which helps with either manual or computer-aided measurement subsequently. However, this is not a required step – see Chapter 7 for further discussion.

(4) Analysis is carried out. For example, if the quadrat method is utilized, particles per cell are counted. Alternatively for the distance method, the distances between particles/aggregates are measured. How the measurements are undertaken will depend on the type of statistical analysis chosen.

(5) Statistical parameters or indices are computed based on the analysis in (10). Parameters such as mean value, deviation, moments and various indices are used to represent the characteristics of materials. Selection of proper parameters to represent the characteristics of material is vital in statistical analysis.

It should be noted that planar images are being assumed. Obviously the fillers are distributed three dimensionally in polymers. Thus, a great effort has been put in predicting the mixing degree in 3D based on 2D data [10,11]. However, at present, only planar arrangements are being considered. Additionally, for particle-polymer composites, there is commonality with the statistical analysis undertaken in ecology, forestry, geography, etc. [12-16] and so forth, which provides valuable references to the statistical analysis of the microstructure of materials.

4.1.2. Dispersion and distribution

The process of ***dispersion*** is to break down agglomerates to aggregates and particles; whereas the process of ***distribution*** is to distribute the aggregates/particles uniformly throughout the polymeric matrix without affecting the particle size [17]. Thus, dispersion and distribution are defined as two independent aspects of mixing. The degree of dispersion is only related to the particle count variation of aggregates and particles, and the degree of distribution is related to the distance between each aggregate/particle. However, in most literature, these two definitions are not distinguished very clearly. However, in the latter part of this chapter, particles in an aggregate are regarded as separate points, and the degree of mixing is only represented by distribution.

4.1.3. Spatial point patterns

In spatial point pattern analysis, points are regarded having no size and are zero dimensional variables. There are three types of spatial point patterns: random, uniform and clustering as illustrated in Figure 4-1 [18].
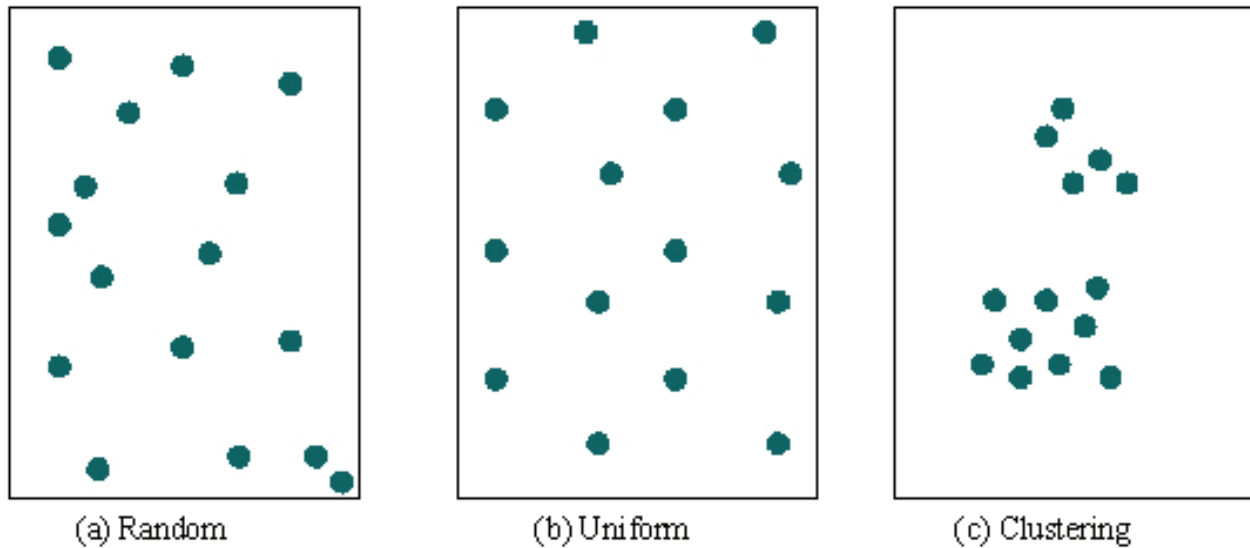
Figure 4-1
Classification of spatial point patterns

In the random pattern, points follow the Poisson distribution, and are equally likely to occur at any location and the position of any point is not affected by the position of any other point. In the uniform or regular pattern, there are repulsive forces between each point, thus they are of the same distance from each other. In a clustered pattern, some points are aggregated and a large portion of areas are left empty or with only few points.

The aim of spatial point pattern analysis is to recognize the pattern to which the object belongs. Several methods, including the quadrat method, the distance method, extended distance method and k-function, are introduced and applied to the analysis of the fillers' dispersion and distribution in a polymer matrix.

4.2. Quadrat method

The quadrat method collects counts of the number of events in subsets of the study region. These subsets could be of any shape but are usually rectangular. Quadrats are placed either randomly or continuously in the study region. A random quadrat is frequently used in ecology or forestry, when the study region is very large and it is possible to study only a small portion of it. A continuous quadrat is used when the whole graph of the study region is available, thus it can be applied to the analysis of the microstructure of materials [17].

There are usually aggregated particles in nanocomposites. An aggregate can be regarded as a point with a characteristic parameter of the number of the gathered particles [19]. The location of the point is the center of gravity of the aggregate. This means that for an aggregate, all the particles aggregated are regarded belonging to the quadrat where the center of gravity of the aggregate is located [7].

4.2.1. Statistical parameters

4.2.1.1. Moment parameters

Statistical parameters such as mean, deviation, higher moments and various indices are used to represent the characteristics of materials.

The nth moment of a probability distribution function $F(x)$ of a real variable, x, is:

$$\mu_n = E(X^n) = \int_{-\infty}^{\infty} x^n F(x) dx \qquad \text{Eq.4-1}$$

where E denotes the expectation. For central moments:

$$\mu_n = E((X - \mu)^n) \qquad \text{Eq.4-2}$$

It should be noted that, the first moment about zero is the expectation of X, which equals the mean value:

$$\mu_1 = E(X - 0) = \overline{X} \qquad \text{Eq. 4-3}$$

The second central moment is the variance:

$$\mu_2 = E(X - EX)^2 \qquad \text{Eq. 4-4}$$

The square root is the standard deviation, :

$$\sigma = \sqrt{\mu_2} = \sqrt{E(X - \overline{X})^2} \qquad \text{Eq. 4-5}$$

The third normalized central moment is termed the skewness which is a measure of the asymmetry of distribution:

$$g_1 = \frac{E(X - EX)^3}{\sigma^3} \qquad \text{Eq. 4-6}$$

The forth central moment is a measure of the peakedness of distribution. Higher kurtosis means more of the variance is due to infrequent extreme deviations, as opposed to frequent modestly-sized deviations. The kurtosis is defined as:

$$k = \frac{E(X - EX)^4}{\sigma^4} - 3 \qquad \text{Eq. 4-7}$$

In quantification of the dispersion and distribution of particles in materials by the quadrat method, the mean value can be regarded as the particle density. The deviation provides information about the difference of individual quadrat counts to the mean value. It is possible to use these two values to quantify the degree of dispersion and distribution. For a particular loading of particles, the particle density of the observed images should be the same. A higher deviation means quadrat counts are quite different from the mean value, which indicates the possible existence of aggregates. For different loadings, standard deviation could be used to quantify the difference with quadrat counts departing from the mean value. This idea is realized in the various indices introduced later.

Skewness measures the asymmetry of the variables' distribution, considering the distribution as measured by the quadrat method. If there are large aggregates, it means that some particles are gathered in a small number of quadrat, while many quadrats are left empty; thus asymmetry in the distribution occurs, resulting in non-zero skewness. Higher skewness indicates a poorer dispersion. Kurtosis is not a proper estimator here. Considering that there is a large peak in the quadrat count, the kurtosis is going to be high since there is a peak, but this does not mean the degree of mixing is uniform or there is clustering since the location of the peak is not reflected in the kurtosis.

Table 4-1
Indices in quadrat method

Index	Name	Estimator
I	Relative Variance	$\dfrac{S^2}{\overline{\overline{X}}}$
ICS	David-Moore index	$\dfrac{S^2}{\overline{\overline{X}}} - 1$
ICF	Index of Cluster Frequency	$\dfrac{\overline{X}^2}{S^2 - \overline{X}}$
$\overset{*}{X}$	Mean Crowding	$\overline{X} + \dfrac{S^2}{\overline{\overline{X}}} - 1$
IP	--	$\dfrac{\overset{*}{X}}{\overline{\overline{X}}}$
I	Morisita Index	$\dfrac{\sum_{i=1}^{n} X_i(X_i - 1)}{n\overline{X}(n\overline{X} - 1)}$
g	Skewness	$\dfrac{N}{(N-1)(N-2)} \sum_{i=1}^{N} (\dfrac{x_i - \overline{x}}{\sigma})^3$

4.2.1.2. Index parameters

The frequently used indices are listed in Table 4-1 [7,17] where X_i denotes the number of particles in the ith quadrat; $\overline{X}$ is the mean of $X_i(i=1,2,...,N)$, S_2 is the sample variance, and   is the standard deviation of X_i. The first five indices are only related to the mean and variance of X_i. The Morisita index and skewness are regarded to be more representative, and have already been used by ecologists [20,21].

Kim et al.[7,22] compared particle density, Morista index and skewness for quantifying the degree of mixing of nanoparticles in polymer nanocomposites. A conclusion was made that skewness is the most effective method to evaluate and compare quantitatively the degree of mixing of filler particles in nanocomposites.

4.2.2. Interpretation of skewness

As is defined by Eq. 4-6, skewness is a measure of the asymmetry of the probability distribution of a real-valued random variable. Usually, an estimator is applied when samples are chosen from a large population:

$$g_e = \frac{N^2}{(N-1)(N-2)}$$

Eq. 4-8

producing the final expression for skewness [7]:

$$g = g_e g_1 = \frac{N}{(N-1)(N-2)} \sum_{i=1}^{N} (\frac{x_i - \overline{x}}{\sigma})^3$$

Eq. 4-9

where N is the total number of quadrats studied, x_i is the number of particles in the ith cell, $\overline{x}$ is the mean value of $x_i(i=1,2,...,N)$.

There are several rules to use this method. First, a proper quadrat size must be determined. Too large a quadrat size will result in roughly the same quadrat count, which will lose information about the dispersion and distribution; while too small a quadrat will result in a considerable number of empty quadrats, which will result in inaccuracy of the estimation. An experiential rule is adopted that the area of the quadrat should be about twice the mean size of all aggregates/particles [7,22]:

$$S_q = L^2 \approx m \square \pi r_{mean}^2$$

Eq. 4-10

where L is the length scale of the quadrat (square quadrat is adopted here), r_{mean} is the mean radius of all aggregates and particles, and m is a constant (approximately 2). For the case of large aggregates, a larger m can be used, usually from 3 to 5. Secondly, for aggregates, if the gravity center is in cell j, then all the particles should be regarded belonging to cell j.

However, for two aggregates/particles, it may be that there is no difference between close arrangement (adjacent but not aggregated so treated separately) and distant arrangement if they belong to different quadrats. An example is provided here. Fig.4-2 shows two simulated micrographs of nanocomposites. If a series $M(x_1, x_2, …, x_n)$ is used to symbolize the particle numbers of aggregates/particles (for particles, it is one), n is the total number of aggregates/particles, x_i denotes the particle count of the ith aggregate/particle. Both Fig.4-2(a) and Fig.4-2(b) have the same degree of dispersion, which means the series M of Fig.4-2(a) and Fig.4-2(b) are the same. However, the aggregates/particles are arranged quite differently, in Fig.4-2(a) they are arranged uniformly; in Fig.4-2(b) they are arranged in a clustered pattern.
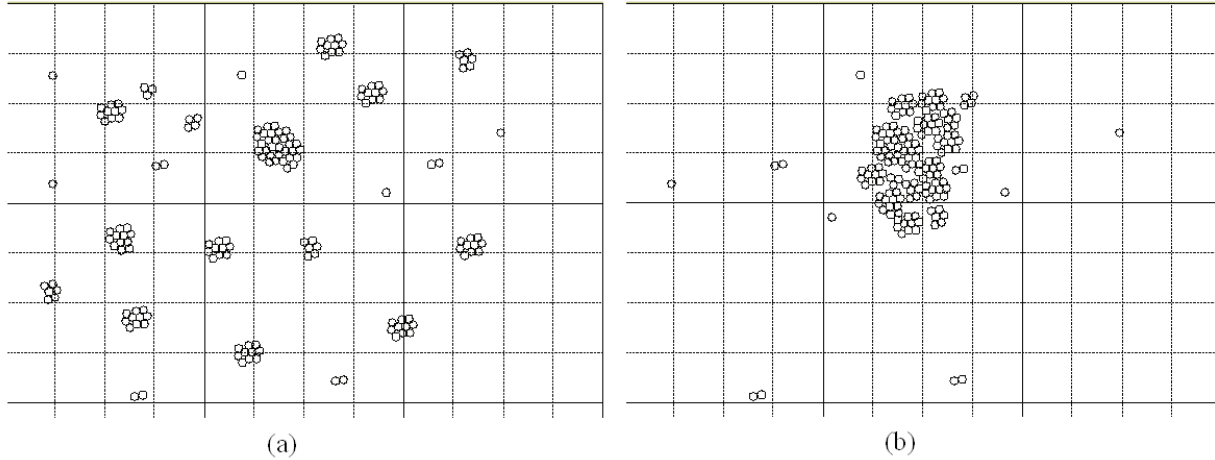
Figure 4-2
Simulated micrograph of nanocomposites with quadrat superimposed

The same quadrat size is used and skewness in the form of Eq. 4-9 is calculated. The skewness for Fig.4-2(a) is 4.1214; while skewness for Fig.4-2(b) is 4.6459 (aggregates counted separately). Skewness can be very large when the particles are poorly dispersed; however, the difference between the two values of skewness is not as significant as the judgment that can be made subjectively in this case. This is an indication that skewness is not very effective for quantifying different distributions.

Another example illustrates the case for different degrees of dispersion, but almost the same distribution shown in Fig.4-3.
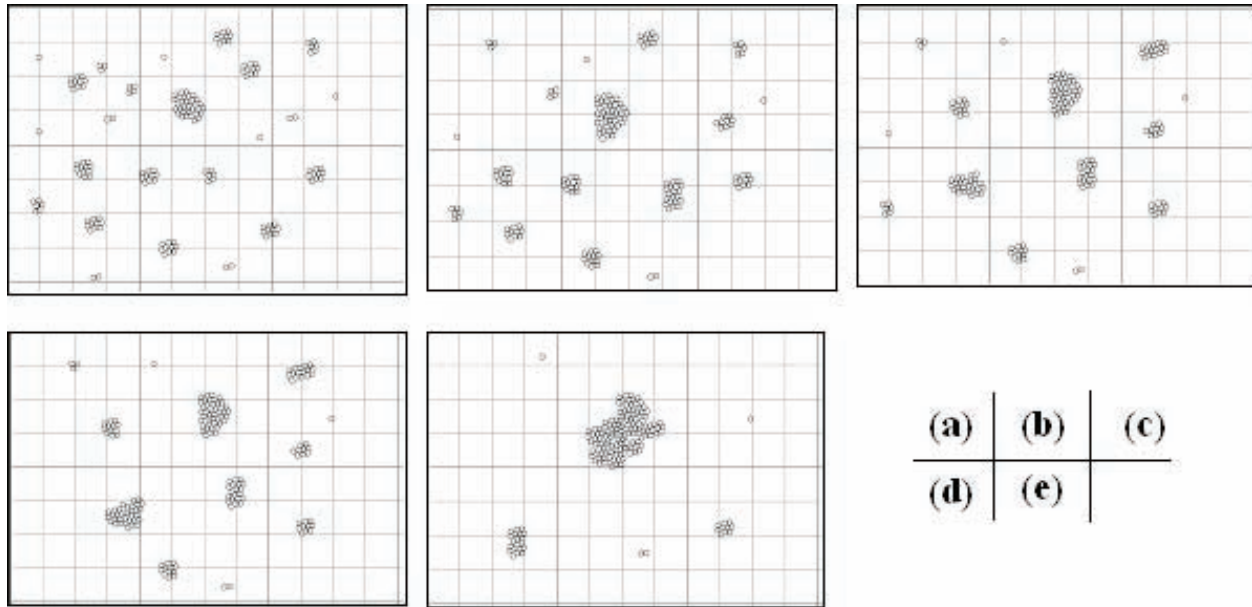
Figure 4-3
Illustration of the same degree of distribution, but different degrees of dispersion

It should be noted that in this example, the same quadrat size is used and the number of particles in every picture is the same. The skewness of the five simulated images in Fig.4-3 will be computed and the results are listed in Table 4-2. Thus, it is obvious that skewness is more sensitive to dispersion, and sometimes can not effectively describe the degree of distribution. It is suggested that other methods should be utilized to quantify distribution which will be introduced in Section 4-3, but skewness is kept to quantify dispersion.

Table 4-2
Skewness for different-dispersed samples

Fig.4-3	(a)	(b)	(c)	(d)	(e)
Skewness	4.1214	5.1937	4.8843	4.8789	9.5375

4.2.3. Normalization of skewness

A skewness comparison cannot be applied directly when the loading in the composites is different. Higher loading will tend to make the quadrat count equal, leading to a smaller skewness. Thus a normalization of skewness for different loadings is needed.

An assumption is made here that, through the normalization process, the degree of dispersion does not change; thus the same quadrat size is applied. Consider initially the unit loading level. A series,

$$C_1: (x_i, i=1,2,\ldots, N)$$

denotes the particle numbers in every quadrat. x_i denotes the particle number of ith quadrat, and N is the total number of the quadrat. Assume there is a non-zero subset Z_1,

$$Z_1 \subset C_1$$

$$Z_1: (x_i, \ i=1,2,...,m)$$

which includes all the non-zero quadrat counts in $C_1(x_i)$. m is the number of non-zero quadrats.

For loading level two, which is twice the loading of the unit loading, a series C_2,

$$C_2: (x_i, \ i=1,2,..., N)$$

denotes the particle numbers in every quadrat. Assume the non-zero subset Z_2 includes all the non-zero quadrat counts in C_2. Due to the fact that, for different loadings, the dispersion is the same, thus assume Z_2 to be equivalent to the sum of two Z_1 series:

$$Z_2 = Z_1 \cup Z_1$$

$$Z_2 : (x_i, \ i=1,2,\cdots,2\times m)$$

For an arbitrary loading level, a, the non-zero subset Z_a is:

$$Z_a = \underbrace{Z_1 \cup Z_1 \cup \cdots Z_1}_{a}$$

$$Z_a : (x_i, \ i=1,2,\cdots,a\times m), \ a\times m \le N$$

The skewness in Eq. 4-9 can be rewritten as:

$$g = \frac{N}{(N-1)(N-2)} \sum_{i=1}^{N} (\frac{x_i - \overline{x}}{\sigma})^3$$

$$= \frac{N^{5/2}}{(N-1)(N-2)} \square \frac{\sum_{1}^{N} (x_i - \overline{x})^3}{(\sum_{1}^{N} (x_i - \overline{x})^2)^{3/2}}$$

Eq. 4-11

Since N is constant, let

$$g_a = \frac{\sum_{1}^{N} (x_i - \overline{x})^3}{(\sum_{1}^{N} (x_i - \overline{x})^2)^{3/2}} = \frac{g_{11}}{g_{22}},$$

$$g_{11} = \sum_{1}^{N} (x_i - \overline{x})^3, \ g_{22} = (\sum_{1}^{N} (x_i - \overline{x})^2)^{3/2}$$

Eq. 4-12

$$g_{11} = \sum_{1}^{N} (x_i - \overline{x})^3 = a\sum_{1}^{m} x_i^3 - 3a^2 \overline{x_1} \sum_{1}^{m} x_i^2 - 2a^3 \overline{x_1}^3 N$$

Eq. 4-13(a)

Let: $P_1 = \sum_1^m x_i^3, Q_1 = \sum_1^m x_i^2$

Therefore, Eq. 4-13 is rewritten as:

$$g_{11} = aP_1 - 3a^2 \overline{x_1} Q_1 - 2a^3 \overline{x_1}^3 N \qquad \text{Eq. 4-13(b)}$$

Similarly,

$$g_{22}^{2/3} = aQ_1 - a^2 \overline{x_1}^2 N \qquad \text{Eq. 4-13(c)}$$

Therefore,

$$g_a = \frac{g_{11}}{g_{22}} = \frac{P_1 - 3a \overline{x_1} Q_1 - 2a^2 \overline{x_1}^3 N}{\sqrt{a}(Q_1 - a \overline{x_1}^2 N)^{3/2}} \qquad \text{Eq. 4-13(d)}$$

However, usually what is known is x_i at loading level a. Again, based on the same assumption:

$$P_1 = \frac{P_a}{a} = \frac{\sum_1^{a \times m} x_i^3}{a},$$

$$Q_1 = \frac{Q_a}{a} = \frac{\sum_1^{a \times m} x_i^2}{a}, \qquad \text{Eq. 4-14}$$

$$\overline{X}_1 = \frac{\overline{X}_a}{a} = \frac{\sum_1^{a \times m} x_i}{a}$$

Therefore, the normalized skewness is:

$$g_{norm} = \frac{N^{5/2}}{(N-1)(N-2)} \frac{P_1 - 3\overline{x_1} Q_1 - 2\overline{x_1}^3 N}{(Q_1 - \overline{x_1}^2 N)^{3/2}} \qquad \text{Eq. 4-15}$$

4.3. Distance method

In spatial data analysis, the distance method measures the distance between points and analyzes the statistical attributes of the measurements. Nearest neighbor methods are frequently employed [19,23,24]. A particle, no matter whether separated or aggregated, is regarded as a single point and the exact location is recorded.
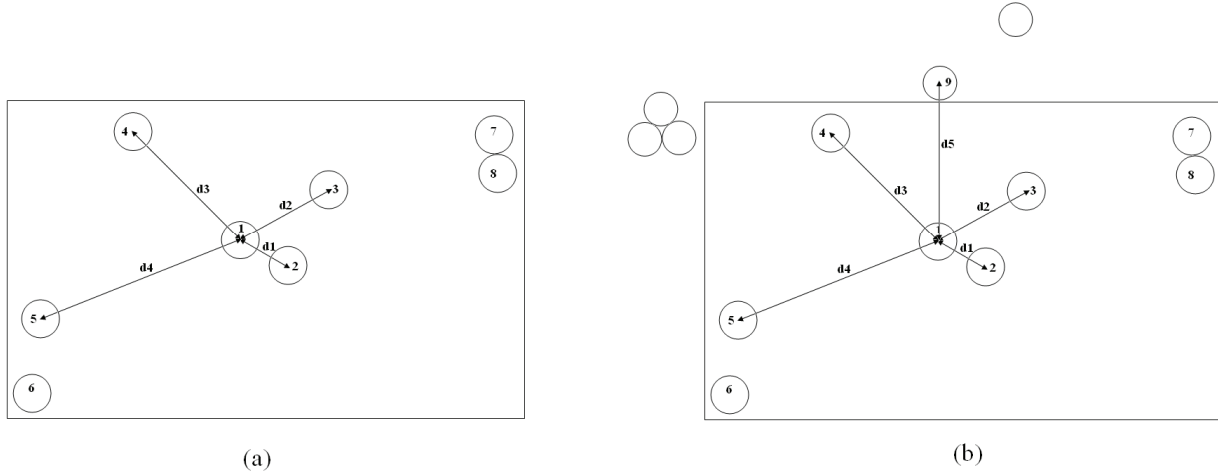
Figure 4-4
Illustration for nearest neighbor method

The points in Fig.4-4(a) symbolize the technique for particles, numbered as 1, 2, …, 8. Distances *d1*, *d2*, *d3* and *d4* are the distances between point 1 to point 2, 3, 4, 5 respectively, and denote the first, second, third, and forth nearest distance of point 1. However, it should be noted that the studied area is only a portion of a larger population. It is possible that beyond the studied area, there exists one point with a shorter distance compared to that within the studied area, as illustrated in Fig.4-4(b). This is called the edge effect. This will lead to the bias of the estimation of the whole population. Therefore, for a reliable measurement of nearest distance, some method should be utilized to correct for this edge-effect. Here, a guarded area method is used which defines an area inside of the studied region [17]. Points inside the guarded area will be the sampling points, and the points outside will not be sampled but counted as the kth nearest neighbor to the points inside. Mean distances of the first, second, third, etc. nearest neighbors can be calculated and compared to the expected distances under complete spatial randomness, extending information on multiple spatial scales.

Consider the distance W_k from an arbitrary event to the kth nearest event, under complete spatial randomness, the expectation is [17]:

$$E(W_k) = k(2k)! / \left\{ (2^k k!)^2 \lambda^{1/2} \right\}, \quad k = 1, 2, \ldots \qquad \text{Eq. 4-16}$$

where   is the particle density. For a study region with an area of *S*, and with n particles within this region, the particle density is

$$\lambda = \frac{n}{S} \qquad \text{Eq. 4-17}$$

Attention should be paid to the density here when edge effect correction is applied. The area should be the guarded area, and the particles should be those inside the guarded area.

From a sample of n events, the kth nearest neighbor distances are calculated as:

$$\{W_{ki} : i = 1, 2, \cdots, n\}, k = 1, 2, \cdots, K$$

The ratio of the sample mean to the expected k^{th} nearest neighbor:

$$R_k = \left\{ \sum_{i=1}^{n} W_{ki} / n \right\} \left\{ (2^k k!)^2 \lambda^{1/2} \right\} / k(2k)!, \quad k = 1, 2, \ldots \qquad \text{Eq. 4-18}$$

The ratios R_k versus k are then plotted to inspect for departures from 1: $R_k > 1$ indicates regularity and $R_k < 1$ indicates clustering, for small k. If points are randomly spaced within clusters, R_k should be less than 1 and approximately constant for small k and should increase as k approaches and exceeds the cluster size. The larger the departure is from unity, the more significant the regularity or clustering.

4.3.1. The first nearest neighbor distance method

The first nearest neighbor distance (also called the mean nearest neighbor distance [23]) makes use of only the first nearest neighbor distance and discards higher order nearest distances. According to Eq. 4-18 the index for the first nearest neighbor distance is:

$$R_1 = \frac{\sum_{i=1}^{n} \dfrac{W_{1i}}{n}}{2\sqrt{\lambda}} \qquad \text{Eq. 4-19}$$

It is possible to inspect the pattern of the distribution by only using the first nearest neighbor distance following the same judgment stated previously. Due to the simplicity of the analysis, it is utilized as the major index when the distance method is applied. However, information of higher order is lost.

4.3.2. The extended distance method and k-function

Extended nearest neighbor distance and the *k*-function make possible that multiple scale information are included instead of only the first nearest index. The extended nearest neighbor distance evaluates a series of the nearest neighbor distances following the expression of Eq. 4-18, and the degree of clustering can be studied with extended information such as the approximate average size of clustering.

The *k*-function is defined as follows [17]:

$$K(h) = \lambda^{-1} \sum_{i=1, i \neq j}^{N} \sum_{j=1}^{N} I(\|s_i - s_j\| \leq h) / N, \quad h > 0 \qquad \text{Eq.4-20}$$

Again, is the particle density and defined by Eq. 4-18. Series $(s_1, s_2, \ldots, s_N)$ denotes all points in the studied region. The function $I(x)$ is the indicator function of x: $I(x) = 1$ if x is true, and $I(x) = 0$ if x is false. The K-function measures the frequency of the points within a circle of radius h, and

divides the total points in the studied region. Under the assumption of complete spatial randomness, $K(h) = \pi h^2$. Under regularity, $K(h) < \pi h^2$, while under clustering, $K(h) > \pi h^2$.

When correction of edge effect is applied to the k-function, Eq. 4-20 is rewritten as:

$$K(h) = \lambda^{-1} \sum_{i=1, i \neq j}^{N} \sum_{j=1}^{N} I(\|s_i - s_j\| \leq h, d_i > h) / N, \sum_{i=1}^{N} I(d_i > h), h > 0 \qquad \text{Eq.4-22}$$

The condition $d_i > h$ confines the distance of the sampled point to the nearest edge is larger than h, to include all the particles within the circle.

4.4. Analysis of real problem

Three micrographs of nano SiO_2-filled XLPE nanocomposites are analyzed. Nano SiO_2 fillers are of nominal radius of r = 12.5nm. Loading levels are 5.0 wt%, 10.0 wt% and 15.0 wt% respectively for the three micrographs in Fig.4-5.
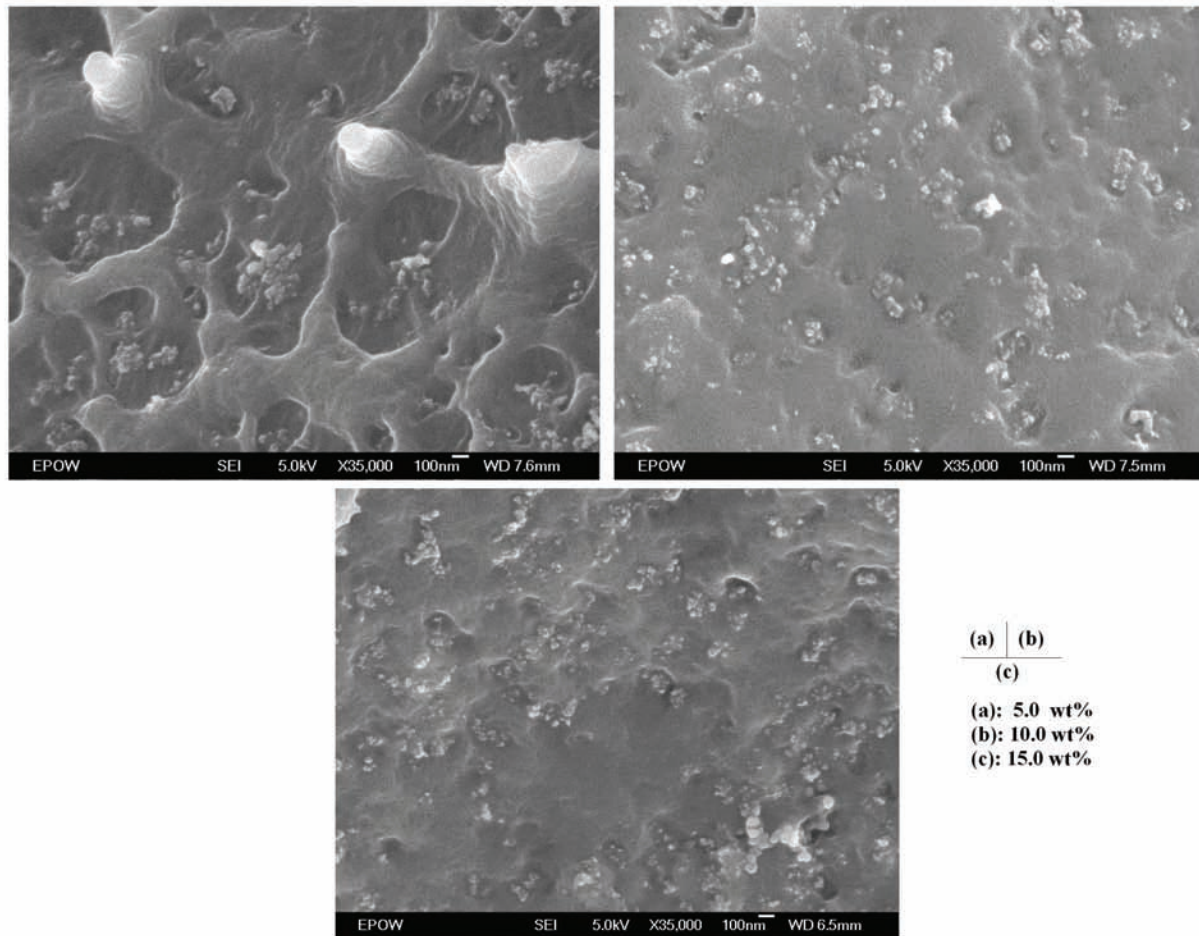
Figure 4-5
SEM images of SiO$_2$-XLPE nanocomposites at different loading levels

Two ways to provide a comprehensive quantification of mixing in independent aspects of dispersion and distribution are proposed.

First, as stated previously, every aggregate is treated as a single point with its gravity center as the recorded location and carries the characteristic parameter of its particle count. The skewness and distance parameters are combined to provide the quantification of mixing, for dispersion and distribution respectively.

Second, all particles, including those aggregated, are treated separately. Here, the distance parameter alone is used to quantify mixing, since the spatial patterns (clustering, uniform and random) are able to describe the mixing level.

4.4.1. Combined skewness and distance measurement

4.4.1.1. Quadrat method based skewness to represent dispersion

A square-shaped continuous quadrat grid is overlaid on SEM micrographs as shown in Fig.4-6. According to the size of aggregates/particles, a fixed quadrat size with a length of 200 nm is used regardless of the different loading level of the three micrographs. Fig.4-7 shows the frequency of quadrat count versus particles per quadrat. The three micrographs all have a considerable preponderance of quadrats with zero counts. Statistical parameters are calculated as shown in Table 4-3, including both un-normalized and normalized skewness.

(a) **(b)**
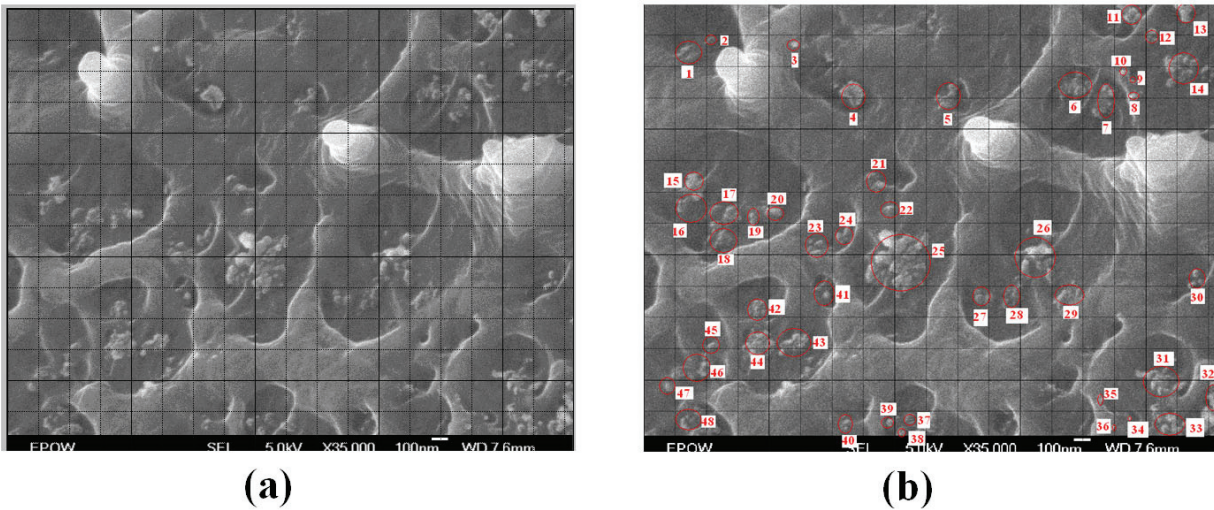
Figure 4-6
Micrograph of SiO$_2$-XLPE nanocomposite at loading level 5.0 wt% with modification according to the different analysis method
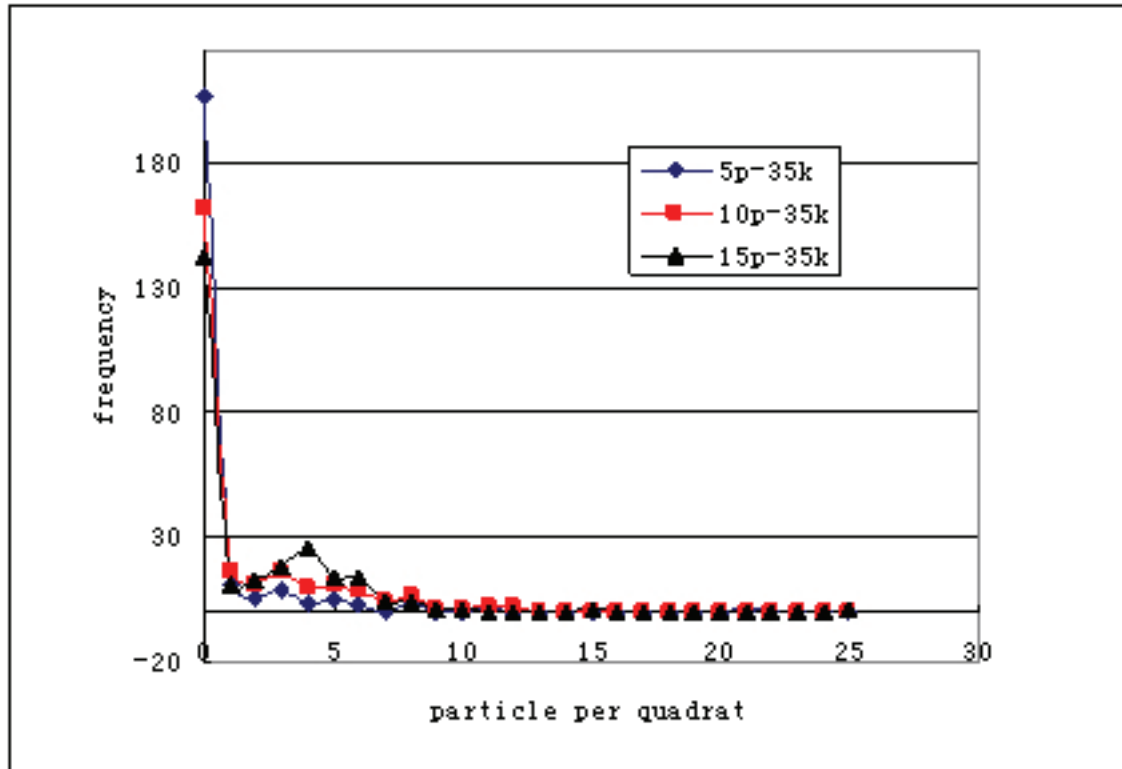
Figure 4-7
Quadrat count frequency distribution

Table 4-3
Statistical summary of SiO$_2$-XLPE nanocomposites

Loading level	Number of quadrat	Particle/ quadrat	Standard deviation	Skewness	Normalized particle/ quadrat	Normalized skewness
a	N	$\overline{X_a}$		g	$\overline{X_1}$	g_n
5	252	0.734	2.205	4.894	0.147	11.250
10	252	1.524	2.622	1.890	0.152	7.672
15	252	1.885	2.908	2.904	0.126	11.692

4.4.1.2. Nearest neighbor distance to represent distribution

In the micrograph of Fig.4-6(b), aggregates are counted as a single point. The (*x*, *y*) location of every point is recorded, the first nearest neighborhood distance is calculated, and the distance index calculated according to Eq. 4-18:

$$R_{5-1} = \frac{\sum_{i=1}^{n} W_{ki}/n}{\left\{(2^k k!)^2 \lambda^{1/2}\right\}/k(2k)!} = \frac{\sum_{i=1}^{n} W_{1i}/n}{2\sqrt{\lambda}}$$

$$n = 48, \quad \lambda = \frac{n}{S}$$

Therefore, $R_{5-1} = 1.022$. Similarly, the first nearest neighbor distance for loading 10% and 15% can be estimated. Both values with and without correction of edge effects are considered. The results are listed in Table 4-4. In Fig.4-8, the first nearest neighbor distances are plotted versus loading percentage. In Fig.4-9, the combined dispersion and distribution is illustrated, with the *x*-axis representing the degree of distribution, and the *y*-axis the degree of dispersion. A high value of *R* denotes a poor dispersion. For the distribution, if the value is less than unity, it indicates a clustered pattern; if the value is larger than unity, it suggests a uniform pattern. Unity denotes random pattern. The nearest neighbor distance is a measurement for the departure from the random pattern. Therefore, a more obvious departure means a more significant pattern of clustering (<1) or uniform (>1).

Table 4-4
The first nearest neighbor distance for SIO$_2$-XLPE nanocomposites with and without edge-effect correction

Loading Level	The first nearest neighborhood distance (without edge effect correction)	The first nearest neighborhood distance (with edge effect correction)
a	R$_1$	R$_1^{'}$
5	1.022	0.928
10	1.082	0.936
15	0.849	0.670
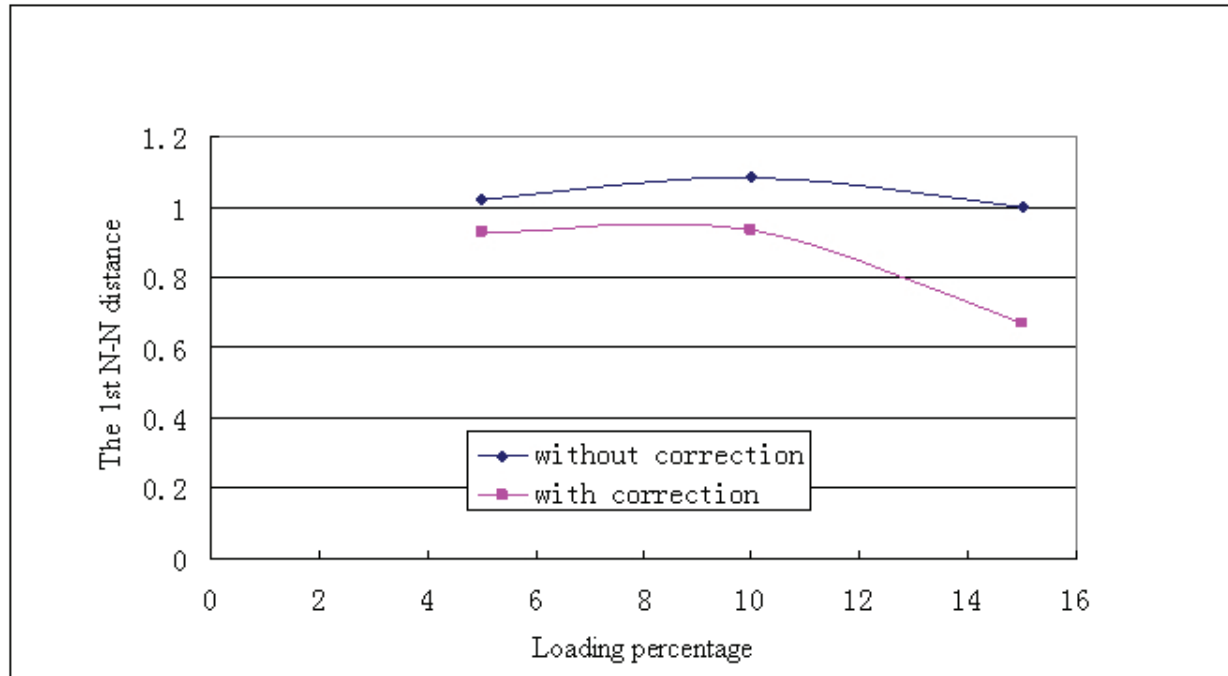
Figure 4-8
The first nearest neighbor distance at different loading levels
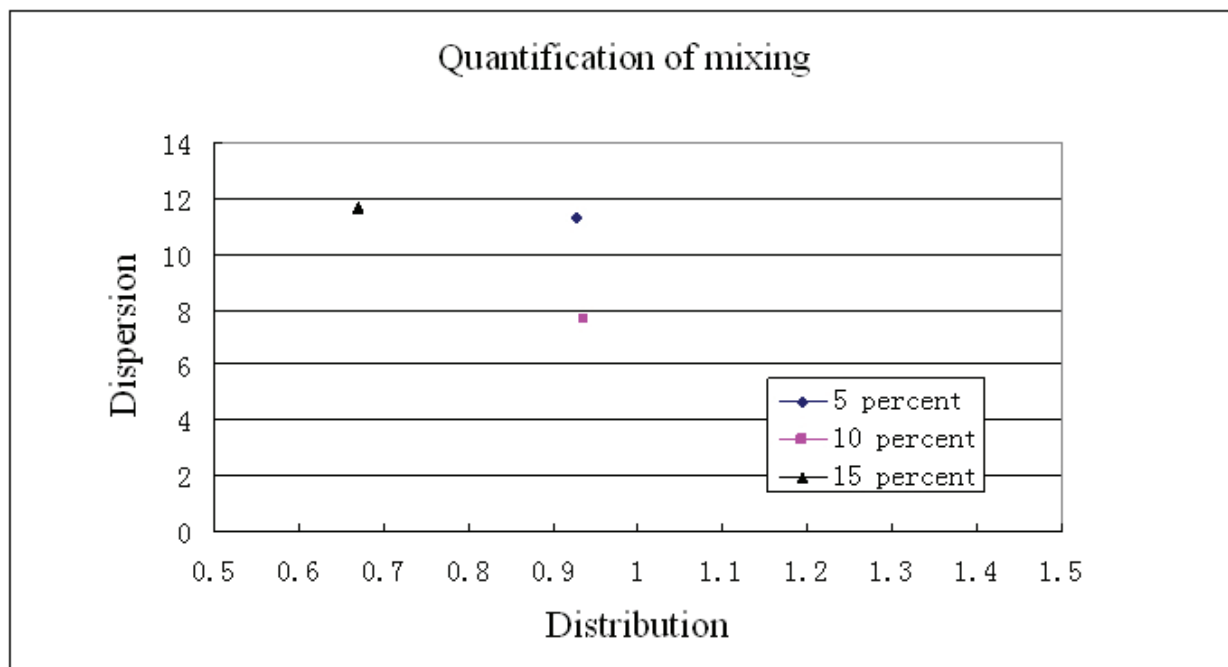
Figure 4-9
Combined dispersion and distribution at different loading levels

From Fig.4-9 it can be seen that, under this quantification method, the 5% and 15% micrographs exhibit roughly the same level of dispersion, which is not as good as that of the 10%. While all three micrographs are less than 1, denoting a clustered pattern; the 5% and 10% cases are very close to 1 and generally of the same degree of distribution. The 15% loading is farther away from unity, indicating a more significant clustering pattern.

4.4.2. Extended distance method and k-function to represent distribution

The micrograph of 5.0wt% loading is analyzed. The exact location of every point is recorded and it is possible to generate a simulated spatial point graph accordingly as illustrated in Fig.4-10.
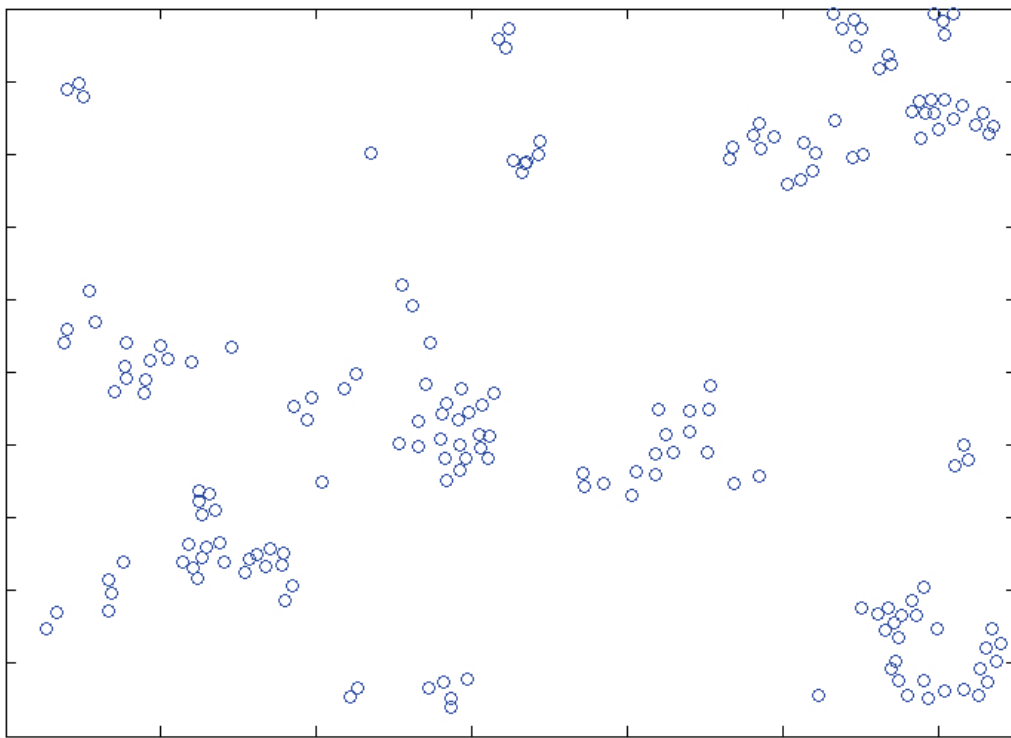
Figure 4-10
Simulated spatial point of the micrograph of SiO$_2$-XLPE at 5.0 wt% loading

Obvious clustering can be observed. The statistical parameters are computed and the kth nearest neighbor distances, following Eq. 4-18, are estimated with and without edge effect correction. The results are shown in Fig.4-11.
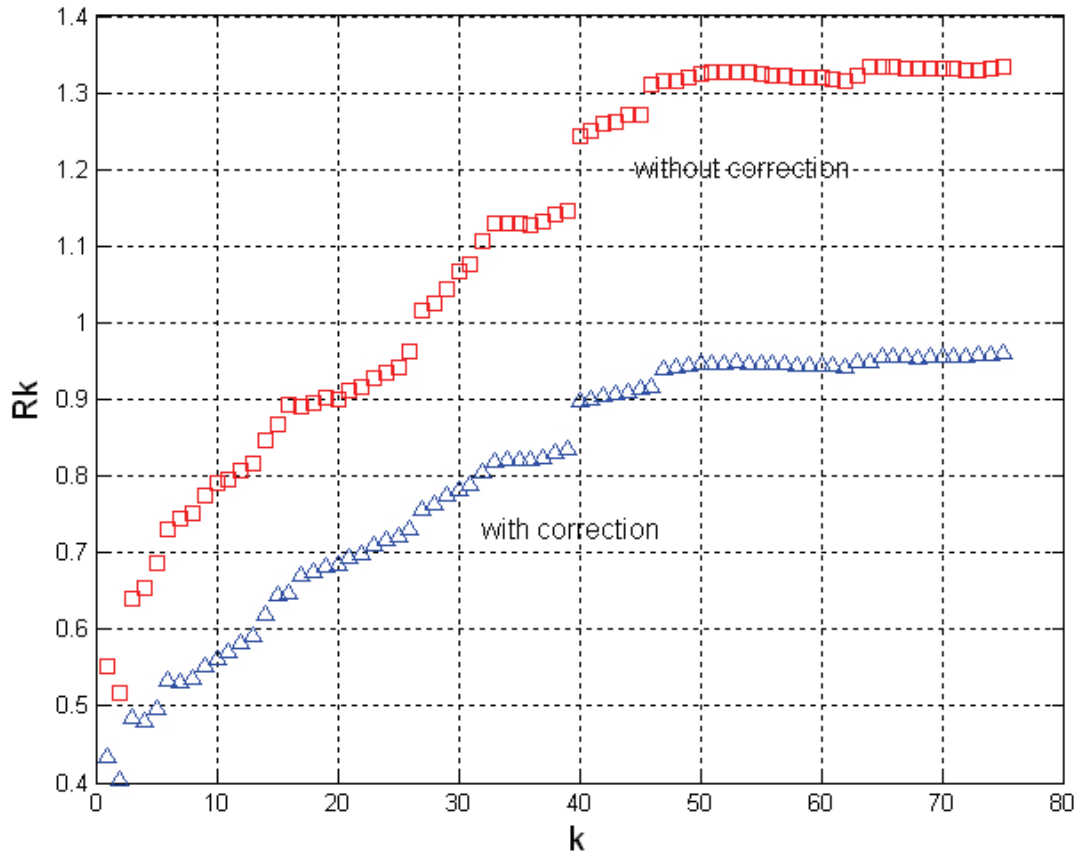
Figure 4-11
The kth nearest neighbor distance with and without edge effect correction

It is obvious that without edge effect correction, the result is biased at higher orders. With edge effect correction, R_k stays below unity and is constant around R_k=0.95 when $k > 47$. At lower k, especially between 1 and 13, the R_k index is relatively small. This indicates an average clustering size of approximately 13 particles, which is in accordance with observation.

The k-functions with and without edge effect correction for the 5.0 wt% loading nanocomposite are computed following Eq. 4-20 and Eq. 4-21 respectively. In Fig.4-12, the *y*-axis is the ratio of *k(h)* to the area of the circle with radius *h*. For smaller *h*, both curves are above 1, which means there is clustering. For larger *h*, the *k*-function without correction exhibits bias. At the same time, the *k*-function with correction equals 1 which is consistent with the fact that for large *h* clustering cannot be observed due to the large area.
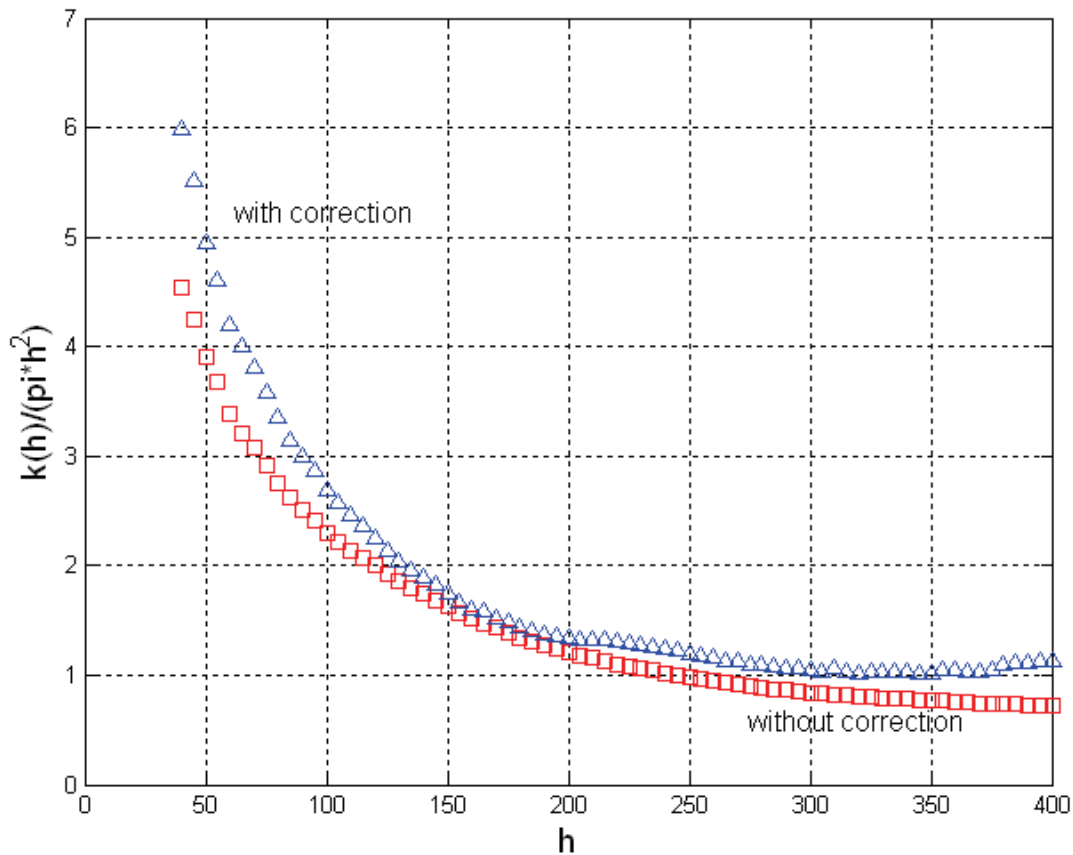
Figure 4-12
***k*-function vs. *h* with and without edge effect correction**

4.5. Conclusion

Spatial point patterns, which are used in forestry, ecology and other disciplines, are applied to the analysis of the microstructure of nanocomposites. Although very different realms, and very different scales, the mathematical essence is the same. The quadrat method, distance method and extended distance method as well as the *k*-function are all possible ways to provide quantification.

Quadrat based skewness is interpreted and found to be more effective in quantifying dispersion. Normalization is realized to make a comparison between different loadings possible. The first nearest-neighbor distance is used to quantify distribution with aggregates counted as a single point. The combination is able to capture both aspects of mixing.

The extended distance method and the *k*-function are able to provide the quantification at multiple scales. Here, particles in aggregate are regarded as separate points, thus distribution alone is able to represent the degree of mixing. Due to the fact that these two methods make use of the exact locations of points, the arbitrariness of choosing the quadrat size is avoided.

However, it is very tedious and time consuming when carrying out the measurement. Computer methods will need to be applied to the statistical analysis. These two methods are able to provide curves instead of indices. Although, the multiple scale values are more comprehensive, the comparison between different materials is easily obtained. As a result, the adoption of such a complex method should be reconsidered. Unless advanced digital image processing is applied to determine the location of every point, these two methods could not be recommended for routine analysis.

Furthermore, the combined skewness and first nearest neighbor distance method makes use of the aggregates which usually exist in composites filled with nano particles, and simplifies the required statistical measurement. Therefore, this method is recommended to quantify the degree of mixing in nanocomposites.

5
PROGRESS WITH MECHANISTIC STUDIES

5.1 Thermally Stimulated Current

Space charge trapping and accumulation is believed [from pulsed electroacoustic (PEA) measurements] to be a major factor in the high-field behavior of dielectrics. For example, as was illustrated in Figure 6-4 of the April 2007 EPRI report [5], the nanocomposite material has a tendency to trap homopolar charge near both its electrodes, and it is felt that this provides a reduced electric field in this region, raising the breakdown strength. The relative depth to which charge carriers become trapped can be seen as they are thermally released from such traps. A thermally stimulated current (TSC) experiment can reveal these trapping depths, and can also give a glimpse into what regions of the materials are responsible for trapping. It is important to note that dipolar relaxations and chain mobility, as well as space charge, contribute to measured TSC. However, the space charge contribution is presumed to dominate at higher fields as charges accumulate in greater amounts.

The test is performed by the creation of an electret by heating a laminar sample of material, applying a poling electric field, then cooling (under field) to a low temperature. The poling field is then removed, and the sample is heated at a constant rate (usually 3°C per minute) with the terminals shorted through a picoammeter. The temperature of the resulting current peaks, along with the slope at which each of these relaxations starts, can be used to determine the location (e.g., amorphous/crystalline interface) and depth, respectively, of the trapping/detrapping mechanism.
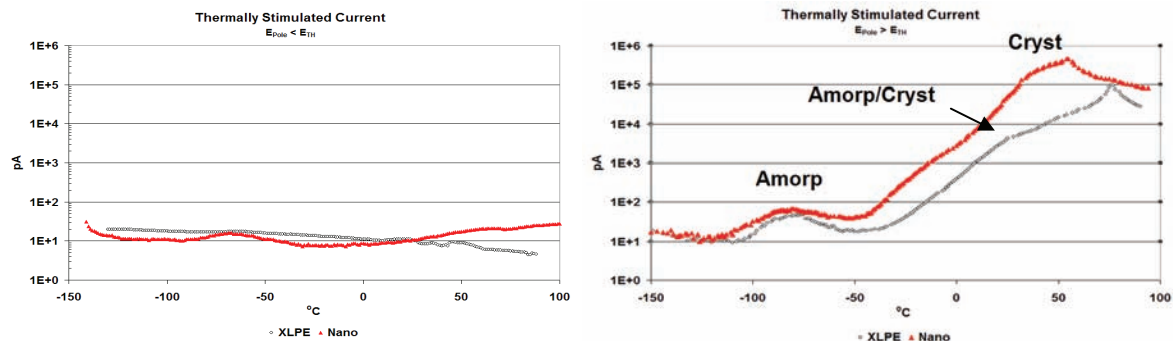
Figure 5-1
Thermally-stimulated current experimental results at a poling field (a) below the threshold of charge accumulation and (b) above the threshold. Poling temperature was 80°C.

Figure 5-1 provides a view of the XLPE and VS-nanocomposite TSC spectra at (a) a low field (10 kV/mm) and (b) a high field (30 kV/mm). The low field case is below the previously-determined charge accumulation threshold for both materials (from the PEA experiment). It is seen in the low field case that the two materials have only weak relaxations, and are in fact very similar to each other in behavior. The activity here is presumably due mostly to dipolar relaxation. The three easily-recognizable peaks of the high field case, on the other hand, are marked with the polymer area likely responsible (in literature on the subject, the polymer regions involved in the location of the temperature peaks have been hypothesized [26]).

Consider the high temperature peaks marked "cryst." This relaxation occurs as the material nears the crystalline melting temperature of polyethylene. It is possible, using the "initial rise" method [27], to fit each peak, those of base XLPE and the 12½% nanocomposite, to a general temperature-activated exponential function

$$i(t) = exp[-E_t / kT] \qquad \text{Eq.5-1}$$

where k is the Boltzmann constant, T is the absolute temperature, and E_t is an activation energy known as the trap depth. Figure 5-2 is a normalized (I/I_{max}) Arrhenius plot of the current in the vicinity of the crystalline peak. On a log-linear scale, the slopes of the initial approaches to the peaks are proportional to the trap depths. It is evident that the nanocomposite has a deeper trapping mechanism at this, the largest, relaxation in the experiment. This is an important point to keep in mind in the understanding of the bulk dielectric behavior, especially at the higher fields.
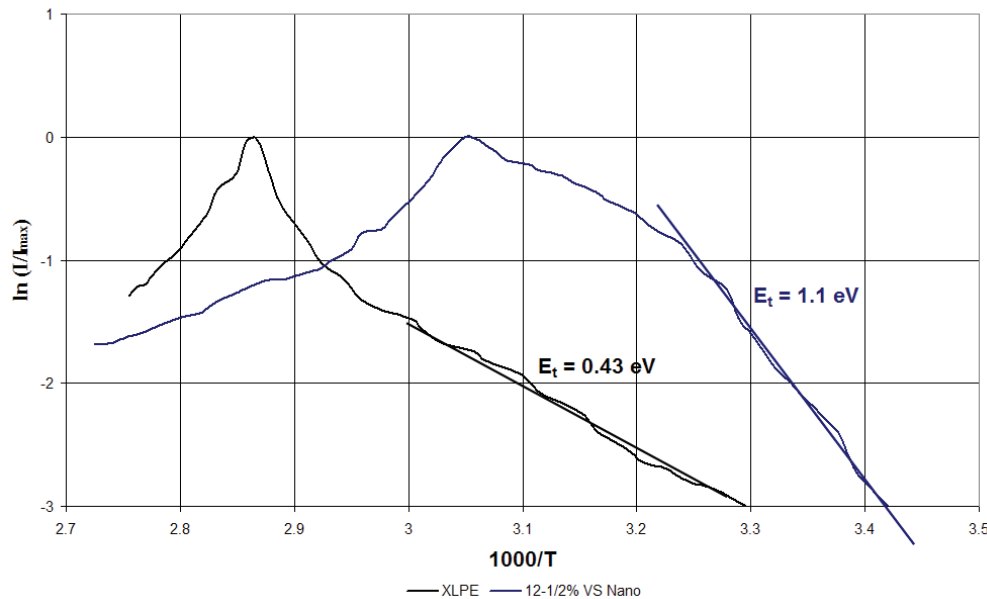
Figure 5-2
Arrhenius plot of the crystalline peaks of Figure 5-1.

5.2 Electroluminescence

The energy of charge carriers is an important consideration in the mechanistic understanding of charge transport in any dielectric material. In order to pursue that aspect, electroluminescence testing of the base XLPE and composites (of two different wt% loadings) was undertaken in the spring of 2007. The experiment consists of applying a DC potential across a highly-divergent field specimen, which causes the excitation of charge carriers. The return of those carriers to their lower-energy states emits packets of energy, *E*, given by the fundamental equation

$$E = h\nu \qquad\qquad\qquad \text{Eq.. } 5\text{--}2$$

where h is Planck's constant and ν is the frequency of the emission. The energy is mostly in the infrared region of the spectrum, and, using optical bandpass filters, can be separated out by wavelength for analysis. Figure 5-3(a) presents the results of the study for the base XLPE as well as 5% and 12½% nanocomposites. The base XLPE has an apparent peak at 400 nm (lower wavelengths mean higher energy), while the nanocomposites' responses are centered about lower energies. Of particular note, the 5% and 12½% nanocomposites have similar behaviors.

Figure 5-3(b) is the corresponding comparison between the base XLPE and the 5% and 12½% microcomposites. Note that the 12½% micromaterial displays the shift to higher wavelength (lower energy), but the 5% micro acts more like the XLPE, with a peak at 400 nm. The two figures together suggest that the lowering of the energy of the carriers is dependent upon the amount of volume that is in the interfacial region between the particles and polymer. Even at the relatively low value of 5 wt%, the nanocomposite, because of the vast increase in interfacial area over the 5% microcomposite, experiences a lowering of its energy while the 5% micro does not. Apparently, a critical value of interfacial volume exists, below which the microcomposite material acts like the base resin.

It is believed that the lowering of the energy in the nanocomposites is due to the presence of charge carrier traps, which are enhanced by the vast amount of particle/polymer interface, and that the traps discourage the attainment of higher kinetic energy by the charge carriers. In addition, the mere presence of the particles themselves may be enough to scatter charge carriers into more arduous and elongated paths, also preventing the higher energies seen in the base resin and 5% microcomposite. However, while this explanation is consistent with many of the desirable properties measured, there are caveats. Firstly, the spectral quality of the emission is dependent on the energy difference between the excited state and a lower level associated with an emission center in the polyethylene which has not yet been identified. While this energy difference is clearly related to the carrier energy of the "hot" electrons, the two measures are not synonymous. It has also been demonstrated [28] that incorporation of nanoparticles into these materials sometimes involves changing the penetration of charge deep into the polymer. It is thus also conceivable that recombination of charge carriers plays a role in the light emission.
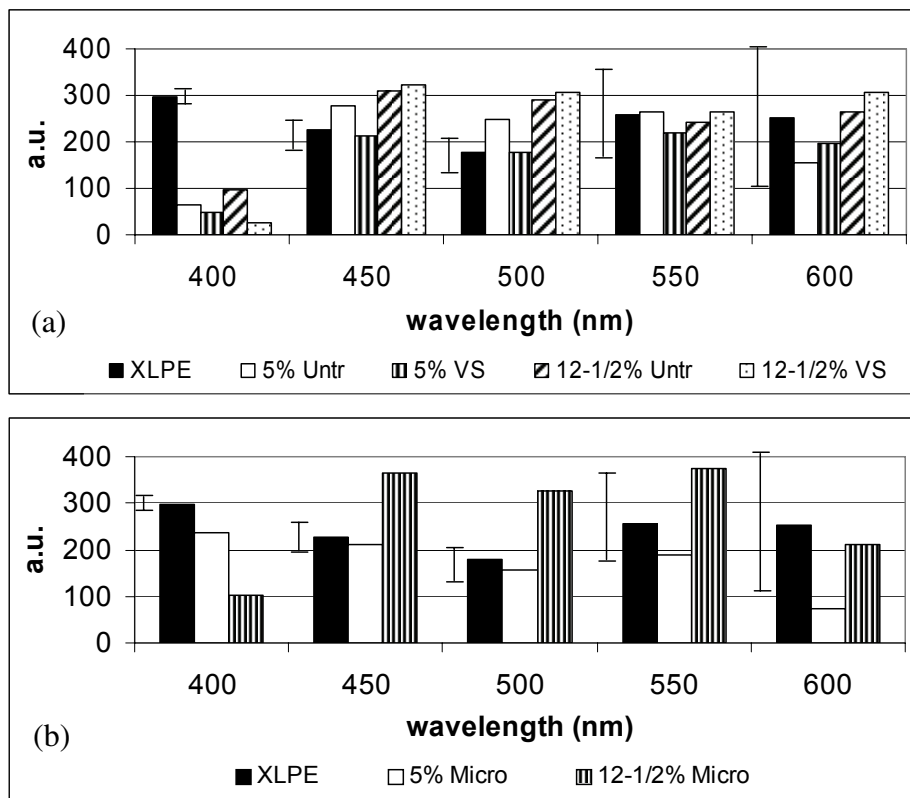
Figure 5-3
Electroluminescence results. (a) Comparison between base XLPE and nanocomposites. (b) Comparison between base XLPE and microcomposites. Maximum electric field (at the divergent-field specimen electrode tip) was 500 kV/mm in all cases.

5.3 Dielectric Absorption Current

To gain further understanding of the different behaviors of the filled and unfilled materials, preliminary absorption current testing has been conducted on XLPE and 12½ wt% microcomposite and nanocomposites (both surface-treated and untreated). The test consists merely of applying a step voltage and measuring the resulting current through each sample as a function of time. Two different applied field intensities were used on the laminar samples: 10 and 30 kV/mm.

Figure 5-4 illustrates the results for the power-on phase of the test, for both the applied field values. A couple of features stand out in these results. Firstly, the behavior of the surface-treated nanocomposite is considerably different at the lower field, which is consistent with the higher threshold of charge injection measured in the PEA space charge test (reported in the April 2007 EPRI report [5], Table 6-1). At the higher field value, the base XLPE and the two nanocomposites behave similarly. Secondly, the microcomposite displays a long time (i.e., low-frequency) onset of conduction behavior which is believed to indicate the migration of charge toward a Maxwell-Wagner interface between the microparticles and the polymer [29]; this is a behavior that is well known for heterogeneous materials generally, but which is mitigated in

nanocomposites. Figure 5-5 of the April report gives corroborating dielectric spectroscopy evidence of this higher loss at low frequencies in the microcomposite [5].
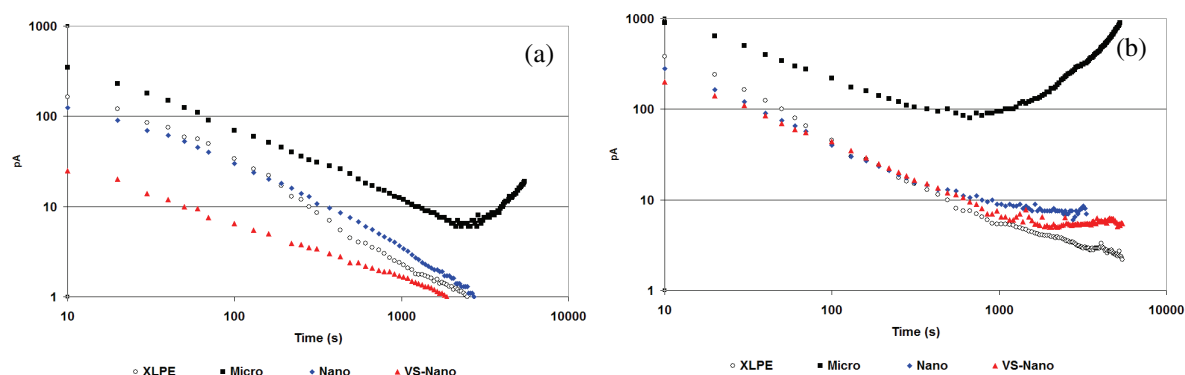
Figure 5-4
Power-on absorption behavior at applied fields of (a) 10 kV/mm and (b) 30 kV/mm (at room temperature).
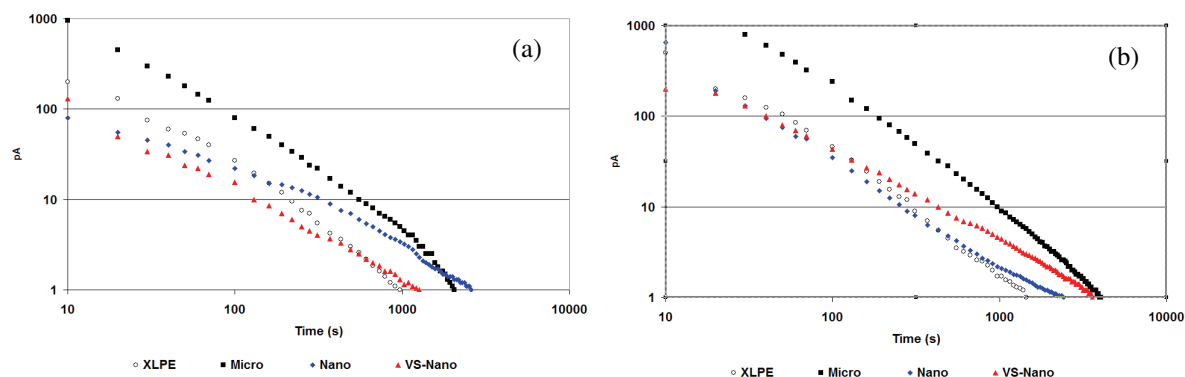
Figure 5-5
Power-off absorption behavior at applied fields of (a) 10 kV/mm and (b) 30 kV/mm.

The power-off (desorption) test also contains useful mechanistic information, and is given in Figure 5-5. The data was collected after a two hour power-on time, with the power supply removed and a short circuit applied to the sample. Once power is removed, the driving forces for charge activity in a material are the permanent and temporary dipoles (which will tend to their randomly oriented states), and whatever space charge gradient was built up during poling. Given that polyethylene is generally non-dipolar, we would expect the dipole relaxation to consist of the migration of charge away from Maxwell-Wagner interfaces to their pre-stressed locations (especially in the microcomposite). Space charge relaxation should only be evident in the 30 kV/mm case since this field intensity (as mentioned earlier) is above the threshold for space charge accumulation, while 10 kV/mm is not.

Jonscher, in his work concerning dielectric relaxation, describes the time domain behavior of materials in the absorption current test according to their exponent *n* in the following empirical relationship [30]:

$$i(t) = At^{-n}$$
<div align="right">Eq. 5-3</div>

where A is a constant. If we consider the 10 kV/mm results in Figure 5-5 (below the charge accumulation threshold, so as not to complicate the analysis of desorption by the introduction of space charge gradient), we can hypothesize about the prevailing relaxation mechanism. Jonscher notes that a "flat loss" condition (i.e., frequency-independent within a certain range), results in a one decade-per-decade decline of current with time, that is, $n = 1$. If $n < 1$, the lumped mechanisms being studied tends toward hopping (i.e., conduction), whereas if $n > 1$, the mechanisms indicate dipolar activity.

Since dielectric spectroscopy has revealed sizeable low frequency activity, the samples immediately prior to $t = 1000$ s are used to calculate *n* for each material, as given in Table 5-1. Interestingly, both the base XLPE and microcomposite show a behavior with a dipolar component. While this was expected for the microcomposite (given that its Maxwell-Wagner characteristics are well known), it is somewhat surprising to see even stronger dipolar behavior in the base XLPE. More importantly, however, is that the nanocomposites essentially display a "flat loss" characteristic in this low frequency region. This is in agreement with Figure 5-6 of the April 2007 EPRI report [5], which does indicate that the loss tangent of each of the nanocomposites is insensitive to frequency at room temperature at low frequencies.

Table 5-1
Time exponent *n* just prior to t = 1000s for the power-off (desorption) phase of the absorption experiment (from E$_{app}$=10 kV/mm).

Material	n
XLPE	1.7
12-1/2% Microcomposite	1.3
12-1/2% Untreated Nanocomposite	1.0
12-1/2% VS-Nanocomposite	1.1

6
THE EMERGING MECHANISTIC PICTURE

In order to place the mechanistic studies in proper context, it is useful to summarize the state of knowledge of nanocomposites and suggest the most likely mechanisms operating to create some of the surprising properties which are seen. This has been assembled here based on prior work in this program and supplemented by selected references from other groups studying primarily spherical, metal oxide nanoparticle filled polymers (such as nanoscale silica/XLPE, titania/epoxy, silica/polyimide, and clay/epoxy [31-40]). Several phenomena have been broadly observed:

   • The measured dielectric constant is often outside the bounds predicted from any of the conventional two-region models [41-45] (Table 6-1) and this inconsistency can partially be rectified using a three-region model developed by Vo and Shi [46] with the interface region having properties different from either the matrix or the particle similar to that depicted in Figure 1-1.

   • There is a consistent increase in breakdown strength upon addition of nanoscale fillers over both the base resin and the micron scale-filled counterpart providing that dispersion is properly controlled [31, 47-50]. Table 6-2 shows results from work with silica in XLPE, titania in epoxy, and clay in epoxy.

   • The partial discharge resistance or endurance strength of nanofilled polymers tends to be at least an order of magnitude higher than for unfilled polymers [51,52].   This has also been found to reflect in an enhanced resistance to surface discharge [52].

   • Dielectric spectroscopy results indicate that in some nanocomposites a local "quasi-conductive" region is present as evidenced by the appearance of classical quasi-DC dispersion at sub-Hz frequencies. This has been shown for untreated silica/XLPE nanocomposites [32]. In others (for example, in aminosilane-treated silica [32]), however, this low frequency dispersion is greatly reduced

   • Space charge studies show that nanocomposites usually exhibit lower and redistributed space charge (Figure 6-1) when compared with conventional composites as well as shorter decay constants (Table 6-3) [53] indicating that the nanoparticle filled polymer dissipates charge much more quickly [41, 51, 54]. This is suggestive of the presence of some very local conductivity and may be explained, perhaps, by quasi-dc conduction as observed for XLPE composites. [32]. However, it is important to recognize that inferences made from the dynamics of internal space charge are not necessarily synonymous with those relying on terminal measurements because of the interstitial polymer. Indeed, it has been found that the local conductivity is not reflected in the bulk resistivity below the percolation limit [47].

Table 6-1
Lichtenecker-Rother predictions of composite material dielectric permittivity (') and measured values at 60 Hz at 25 °C [41-43], at 30 °C [44]

Material	f(Hz)	ε'(L-R)	Measured ε'
Unfilled ether-bisphenol epoxy resin	1k	----	10.0
Untreated 23 nm nanotitania	1k	----	99
10 wt% (3.0 vol%) untreated 22 nm nanotitania-filled epoxy resin	1k	10.1	13.8
Unfilled polyimide (BTDA-ODA)	100k	----	3.5
Untreated 12 nm nanoalumina	100k	----	9.8
5 vol% untreated 12 nm nanoalumina-filled polyimide	100k	3.7	6.0
Unfilled crosslinked polyethylene (XLPE)	100k	----	2.4
Untreated 12 nm nanosilica	100k	----	4.5
5 wt% (1.9 vol%) untreated 12 nm nanosilica-filled XLPE	100k	2.4	2.0
Unfilled low-density polyethylene (LDPE)	10k	----	2.3
Untreated 30 nm ZnO nanoparticles	10k	----	8
10 wt% (1.7 vol%) untreated 30 nm ZnO nanoparticle-filled LDPE	10k	2.35	2.52

Table 6-1
Breakdown strength for unfilled and nanoparticle-filled resins showing that the addition of nanoparticles increases the dielectric breakdown strength. The Weibull shape parameters are given in parenthesis.

Material [Ref]	dc Characteristic Breakdown Strength @ 25°C in kV/mm (β)	dc Characteristic Breakdown Strength @ 80°C in kV/mm (β)
Unfilled XLPE [31]	270 (2.5)	79 (3.8)
5 wt% untreated 12nm nanosilica-filled XLPE [31]	315 (2.0)	83 (3.1)
5 wt% vinyl silane-treated 12nm nanosilica-filled XLPE [31]	446 (1.7)	220 (2.9)
Unfilled ether-bisphenol epoxy resin [24]	332 (10.56)	------
10 wt% untreated 22 nm nanotitania-filled epoxy resin [49]	391 (10.39)	------
Unfilled ether-bisphenol epoxy resin [50]	347	------
4-1/2 wt% nanoclay (MMT)-filled epoxy resin [50]	531	------
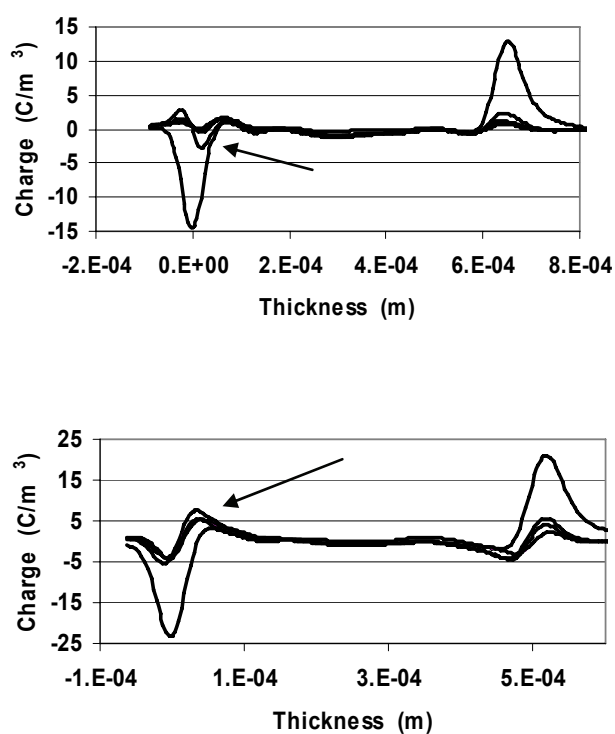
Figure 6-1
The distribution of space charge in a polled 10% titania/epoxy nanocomposite (top) and microcomposite (bottom). The cathode is on the left. The nanocomposite plot indicates the presence of homopolar charge adjacent to the cathode, while the microcomposite's charge near the cathode is heteropolar (arrows) [53].

Table 6-2
Exponential time constant of polarization and space charge decay from the PEA experiment [53].

Material	Polarization Decay (s)	Space Charge Decay (s)
Unfilled ether-bisphenol epoxy resin	40	4800
10 wt% 1.5 µm microtitania-filled epoxy resin	90	6300
10 wt% untreated 22 nm nanotitania-filled epoxy resin	24	2210

6-3

6.1 Mechanistic hypothesis of the part played by the interface

These exciting results for polymer nanodielectrics have led to several hypotheses about the mechanism creating the improved properties [31,53,55]. They all emphasize the critical role of the interfacial region. This section brings together the literature in this area and presents a working hypothesis for the multiscale phenomena operating in polymer nanodielectrics. The reader should recognize, however, that some of this insight is currently somewhat speculative. Consider first a physical depiction of the interface region (Figure 6-2). In thermoplastics the interfacial polymer can exhibit changes in crystallinity [56, 57], mobility [58], chain conformation [59], molecular weight [60], and chain entanglement density [61]. For amorphous polymer systems, the mobility of the polymer chains has been found to increase when the matrix/particle interactions are attractive and decrease when the interactions are repulsive [58]. The size of the interfacial region in this case is about the radius of gyration of the polymer chains (10-20 nm). Within this region, there may be more tightly bound and loosely bound regions, and it is clear that there is a continuous change in structure and mobility (Figure 6-2). In crosslinked matrices such as the XLPE of interest here, there is an additional complication of changes in crosslink density [61] due to small molecule migration either to or from the interface. There is also direct experimental evidence showing some change in the free volume in the interfacial region [62].

It is also important to picture the interfacial region in terms of its ability to directly impact dielectric properties. Tanaka recently developed a multi-core description that tries to capture the charge behavior and structure of the interfacial region [62]. Superimposed on the structural and mobility gradient described above is a charged region. The metal oxide nanoparticle has a surface charge (due to the differences in Fermi level between the filler and polymer), that creates a Stern layer at the 2D interface. This is screened by a charged layer in the polymer. There are compelling arguments to suggest that the next layer is a diffuse double layer of charge (also depicted in Figure 4) with • 10 nm of radial depth in a resistive medium not unlike the ionic Gouy-Chapman layer associated with liquid interfaces [63]. Since this is a region of mobile charge, it has a significant influence both in the dispersion of nanoparticles and in the resulting dielectric and conductive properties of the composite. Note, therefore, that if the charge distribution on the surface of the metal oxide particle is altered either through coupling agents or through the type of bonding, then this layer will also be altered by the interface. In addition, due to the altered charge, altered mobility, and altered free volume, there is the potential for changes in the trap site density as well as depth.

It is well understood from the literature that the polymer structure and dynamics can vary in the presence of a nanoparticle surface. This is shown through changes in the glass transition temperature [64.65], crystalline structure [66] organization [67], and polymer rheology [68]. In addition, for a non-ideal interface there will be surface states. When carriers are provided from the bulk to fill these states the adjacent material become charged, and the energy bands are bent as depicted in Figure 6-4. In the case of nanoparticles, this surface area of contact with the polymer is dramatically increased and thus it is reasonable to assume that there is a large volume of polymer with altered charge distribution in the vicinity of the nanoparticles.

Based on this picture of the interface, the hypothesis for the impact of the interfacial region on dielectric properties is summarized as follows:

    (a) The nanoparticle surface creates a change in polymer structure (free volume, mobility, etc.) and local charge distribution.

(b) As the size of the filler is reduced, the interfacial region becomes dominant.

(c) Due to the change in local structure, the density and perhaps the depth of trap sites are altered which reduce carrier mobility and energy.

(d) If the carriers are trapped more often, then they are accelerated over shorter distances and have reduced energy. This is the same for carriers that are scattered. This causes less damage in the material and increases the lifetime of the polymer.
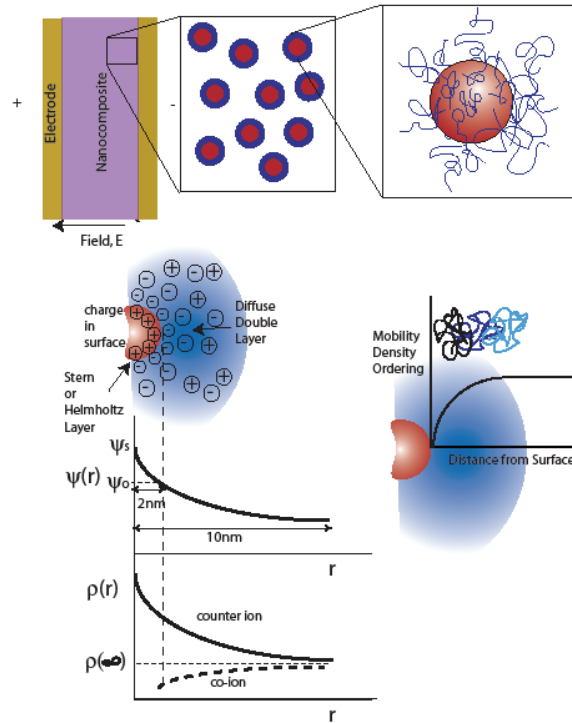
Figure 6-1
A schematic showing that the dielectric properties need to be considered at the macro scale, meso scale, and molecular scale followed by an image of the changes in structure and charge distribution near a particle surface.

(e) The homocharge resulting from carrier trapping mitigates the electric field at the electrodes and increases the voltage required for charge injection. This increases the voltage required for short term breakdown. Because this charge takes time to build up, the breakdown strength is a function of the rate of measurement (ac, dc, or impulse).

(f) The large interfacial area also creates opportunities for increased scattering. During impulse test conditions, this may become the primary mechanism for the increase in the breakdown strength of nanocomposites, since significant shielding homocharge cannot be accumulated in such a short time.

(g) The diffuse layers of mobile charge create <u>local</u> conductivity, which can serve to reduce charge accumulation, providing that the percolation limit has not been exceeded so that the bulk conductivity is unaffected.

Because the interfacial area is so large, while some of these mechanisms may operate in micron filled composites, they are then overshadowed by the large defects the micron scale fillers introduce and the field enhancements they create. Microcomposites exhibit Maxwell-Wagner interfacial polarization which is generally absent in nanomaterials.

6.2 Evidence for SiO$_2$-polyethylene nanocomposites

While the hypothesis advanced in Section 6.1 is general, much of the evidence for it does come from the silica/XLPE system under study here, specifically a commercially available low-density polyethylene melt blended with silica powder (of nominal particle sizes 6 μm and 12 nm [micro and nano]). The processing has been described in Section 2.1 and elsewhere [69], and the functionalized particles were provided with a surface treatment of triethoxyvinylsilane vapor (all microsilica used in this work was <u>not</u> surface-treated). The concentration of triethoxyvinylsilane is less than one monolayer, but has not been quantified.

6.2.2 Charge mobility

Absorption current tests (Figure 5-4) were performed on 12½ wt% silica/XLPE to evaluate the relative ease with which charge fronts propagate through the material bulk. When a dc field is applied to a finite thickness of non-ideal dielectric sandwiched between two plane parallel electrodes, the current decays with a power law dependence {Eq. 5-3}. When a charge front arrives at the electrode, there is a change in slope of the current with time. The mobility, μ, can be calculated from the time it takes the front to reach the electrode, or the transit time, t_t through a dielectric's thickness, d, under an applied voltage, V, using [70]

$$\mu = \frac{0.79 \cdot d^2}{t_t \cdot V}$$

Eq. 6-1

From such measurements it has been demonstrated [43] that the charge carrier mobilities in nanocomposites are both significantly lower than those in polyethylene and also decrease with the applied field.

Absorption current measurements provide clear evidence of carrier trapping in nanodielectrics.

Material	Current Decay Exponent n
Unfilled XLPE	1.34
12-1/2 wt% 6μm micosilica-filled XLPE	1.49
12-1/2 wt% untreated 12nm nanosilica-filled XLPE	1.04
12-1/2 wt% vinyl silane-treated 12nm nanosilica-filled XLPE	1.05

Initially, both the XLPE and the nanocomposite display the classic $I(t) \propto t^{-n}$ shape until the charge front arrives at the electrode, at which time there is a demonstrable change in the slope. For XLPE, this takes place at approximately 500 s, while for the composite it occurs at nearly 1000 s, indicating that charge mobility has been reduced by a factor of 2. The increased number of trap sites would cause the electrons to be accelerated over shorter distances. This would decrease their energy (and thus their ability to create damage in the polymer). Additional absorption data from the depoling phase (following 90 minutes of poling, the voltage supply was removed and a short circuit applied for an additional 90 minutes) allows calculation of the current decay exponent, *n*, for each material, summarized in Table 6-4. Thus, for example, the decay of XLPE takes place at 1.34 decades of current for each time decade; this value is higher for the microcomposite but considerably smaller for the nanocomposites. This is in agreement with the scattering/reduced mobility hypothesis.

Table 6-3
Current decay from the depoling phase (Following 90 minutes of poling at 30 kV/mm) of the absorption current experiment (decade/decade)

6.2.3 Trap site density

The thermally stimulated current (TSC) measurements of Figure 5-1 were used to investigate the nature and origin of charge carrier traps. On account of the large interfacial volume there is a change in the density of trap sites (and perhaps their depth). The TSC measurements indicate a change in the density and perhaps the depth of the trap sites. While the interpretation of TSC relaxation data for semi-crystalline polymers such as polyethylene is more complicated than that for purely amorphous materials, one feature does stand out here. There is an enhancement of the relaxation peak above room temperature, (the so-called alpha peak) by a factor of at least 3. This is due to an increase in the number of charge trap sites (and thus an increase in the thermally-assisted relaxation that can occur). Thus, during poling, more charge carriers were captured in trap sites, and during the subsequent heating phase, more charge carriers were thermally excited into the conduction band.

6.2.4 Pulse electroacoustic analysis

This picture is further supported through PEA measurements [3,4]. Figure 6-3 illustrates the space charge condition for the base XLPE, microcomposite, and vinyl silane surface-treated nanocomposite. A series of PEA experiments had previously been performed [3] to determine the threshold electric field intensity for charge injection, and each curve in the figure was obtained under the same multiple of that threshold. While the base XLPE displays a region of cathode-shielding homocharge extending nearly to the anode, and the microcomposite contains some field-strengthening heterocharge near both electrodes, the plot indicates the presence of shielding homocharge at both electrodes for the nanocomposite material. This may be further evidence of increased trapping of charge and/or scattering. Homocharge injected by the cathode in XLPE (which, from the absorption current experiment, was seen to be relatively free to move) appears to have migrated all the way to the anode, where some recombination could have occurred with space charge there. Similarly, the microcomposite's heterocharge regions may be a result of electron migration from the cathode. However, the nanocomposite maintains two distinct regions of
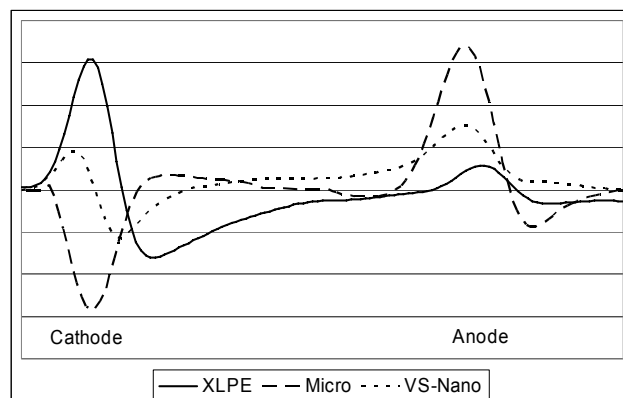
Figure 6-2
Space charge profiles from the PEA experiment 10 seconds after power-off. The nanocomposite has a region of homopolar charge near both electrodes.

homocharge, indicating its lack of mobility for injected space charge under the influence of the electric field.

6.2.5 Dielectric strength

Evaluation of short-term ac (60 Hz), dc, and impulse dielectric breakdown strength and longer-term voltage endurance has been performed on the materials [both EPRI reports]. The dc and ac (60 Hz) breakdown testing data is summarized in Table 6-5. For all the materials tested (base XLPE and 12½ wt% micro, untreated, and vinyl silane-treated nanocomposites) the dc test provided higher breakdown values than did the peak values of the ac test, suggesting that the breakdown mechanisms involved are all related to the rearrangement of charge distributions, which would be mitigated every half cycle in the ac test. Additionally, the surface-treated nanocomposite material demonstrated a significantly higher dc strength than its untreated counterpart, but only slightly higher in the ac test. This suggests that the different bonding structure at the surface of the particles changes the effectiveness of the interaction zone such that its reach into the surrounding polymer structure is perhaps increased for the treated material.

If the clustering of homocharge near the electrodes due to trapping sites were the only mechanism responsible for the electrical enhancements seen in nanocomposites, one would expect to see no improvement (or practically none) when comparing the different materials in the impulse breakdown

Table 6-4
Breakdown strength for filled and unfilled XLPE showing that the addition of nanoparticles increases the dielectric breakdown strength. (The Weibull shape parameters are given in parenthesis).

Material	dc Characteristic Breakdown Strength @ 25ºC in kV/mm (β)	ac (60 Hz) Characteristic Breakdown Strength @ 25ºC in peak kV/mm (β)
Unfilled XLPE	184 (5.1)	178 (4.5)
12½ wt% 6μm microsilica-filled XLPE	162 (5.9)	139 (5.4)
12½ wt% untreated 12nm nanosilica-filled XLPE	191 (4.8)	186 (5.0)
12½ wt% vinyl silane-treated 12nm nanosilica-filled XLPE	239 (5.2)	193 (5.8)

test. After all, PEA testing reveals that the time required for significant accumulation of space charge in the bulk of the test specimens is in the tens of seconds or even several minutes. The impulse test is completed in microseconds; thus little or no improvement would be anticipated. However, Table 6-6 indicates that this is not the case. Indeed, the breakdown field under impulse conditions is

Table 6-5
Impulse test breakdown fields for the XLPE and 12-1/2% nanocomposite materials. The Weibull shape parameters are given in parentheses.

Material	1.2x50 μs Impulse strength @ 25 ºC in kV/mm (β)
Unfilled XLPE	254 (3.6)
12½ wt% untreated 12nm nanosilica-filled XLPE	311 (4.9)
12½ wt% vinyl silane-treated 12nm nanosilica-filled XLPE	332 (5.2)

significantly raised in the nanocomposites.   With the accumulation of space charge ruled out, it appears that the presence of the nanoparticles and the important interaction zones present an elongated scattering path to the charge carriers, such that the initiation of breakdown-level conduction current requires a higher electrical impulse field. Consequently, a likely scenario is that both scattering and homocharge near the electrodes contribute to the enhanced electrical performance of nanodielectrics.

6.2.6 Voltage endurance

A comparison of the AC voltage endurance for the base XLPE and the 12½ wt% surface-treated nanocomposite has been documented [32]. The XLPE is outperformed by the nanocomposite, most likely due to reduced carrier energy, which in turn is a result of the increase in trap sites in the nanocomposite as discussed earlier. Since the initiation of electrical trees within the material involves bond breaking by hot electrons, it follows that reduced carrier energy (as suggested later in the electroluminescence test results) would result in improved voltage endurance. Note that no

voltage endurance testing of the microcomposite system has been undertaken since, according to [47] and other literature on the subject, metal oxide filled microcomposites exhibit a reduction in voltage endurance over similarly weight-filled nanocomposites. This is not to imply that microparticles do not, in some circumstances, exhibit improved voltage endurance properties over base resins. One need only look to the use of silicates in insulating tapes for electrical machine windings as a common example of conventional fillers being used for voltage endurance improvement [71].

6.2.7 Electroluminescence

Evidence for a decrease in carrier energy also comes from the electroluminescence results. The rough spectra shown in Figure 5-3 suggests that the energy of the carriers has decreased for all the nanocomposites. As discussed in Section 5-2, it appears that the spectral shift occurs when a critical interfacial area is introduced and this can also occur with micron scale composites, but at higher loadings. This concept of a critical interfacial area suggests that nanocomposites of very small loadings (even less than 1 wt%) would still see the shift in energy since the interfacial area of such a nanocomposite still exceeds that of a microcomposite of several wt%. This behavior is not limited to the XLPE system. Prior work in titania-filled epoxy also showed that the nanofilled composite shifted to a higher wavelength (lower energy) at 10 wt% and the micron filled did not [53]. This suggests that the polymer structure is not key to the trapping mechanism, but that the charge layer that develops between the metal oxide and the polymer is the most critical. Thus a picture is emerging of an increase in trap sites in the nanocomposites that leads to decreased charge mobility and lower energy of the carriers.

7
CONCLUDING REMARKS

This is an interim report since the work is still ongoing. The tasks described have been undertaken in tandem and thus there is still work to be continued in order to complete most of the tasks.

7.1 Consistency during scale-up

The technology transfer aspects of the program have centered on using the AC dielectric strength as a measure of the efficacy of the technology. This has been undertaken at both Rensselaer (using recessed specimens) and at Dow Chemical using unguarded laminar samples. Although tests at Rensselaer typified by Table 3-1 continue to show improvements in dielectric strength up to a loading of 12 ½%, this is not always seen in tests conducted at Dow Chemical. An example is shown in Figure 7-1 (courtesy of Dr. J. Han) which actually depicts a somewhat smaller electric strength (expressed in V/mil) for the nanocomposite than for the base polyethylene when prepared by either method. There seems to be no good explanation for this at present and is somewhat surprising since it is understood that the correct improvement is seen when the materials are extruded and not molded. It may result from poor dispersion. Before agglomeration was properly mitigated, early results at Rensselaer also showed this tendency. It is certainly well know that the quality of the dispersion is a key factor in the performance of nanocomposites.
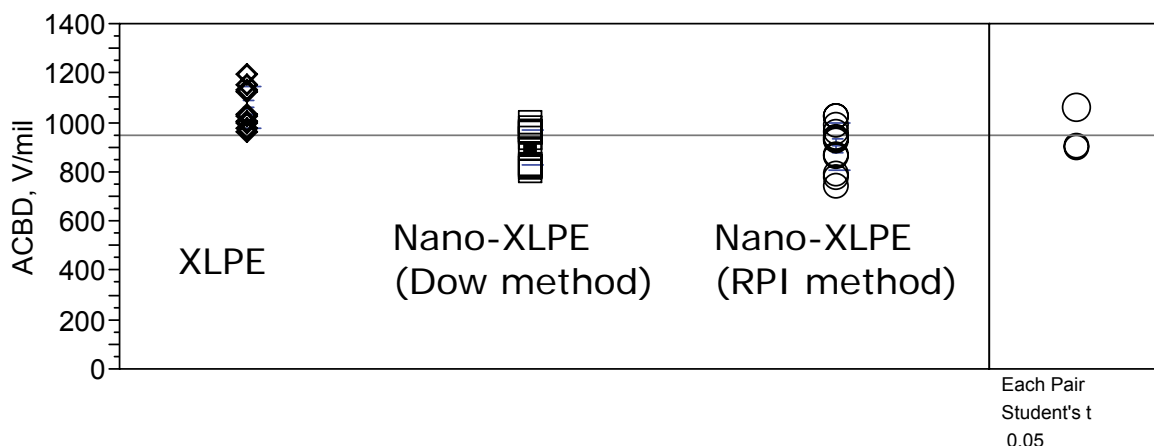

Figure 7-1
AC Breakdown strength of vinylsilane-treated SiO$_2$ nanocomposite in comparison with the base resin.

At the present time, mixing of a lower weight percent nanocomposite at RPI has been proposed, with the resulting material shared between RPI and Dow for independent breakdown testing, to further investigate and verify consistency between the two facilities' test methods.

It is the need to quantify the dispersion which led to the work described in Section 4. While this provides a basis for the description of both dispersion and distribution, it is currently a manual and very time consuming analysis. As the work proceeds, it is planned to attempt the use of recognition software to automate the process. This will be attempted using the ***ImageJ***[®] image processing software platform, which can process digital images and carry out certain measurement and statistical analysis. In this way, the automation of the analysis of Transmission Electron Microscopy (TEM) images will make it possible to obtain the coordinates and the area of particles/aggregates automatically. Consequently, the combined skewness and distance method described in Section 4 can then be applied directly. Using the ***ImageJ***[®] software it should be possible to measure every nano particle in the image automatically, permitting multiple scale information using the extended distance method and k-function.

In preparation for this, arrangements are being made to transition onto the transmission electron microscope to permit better resolution. However, ***ImageJ***[®] also provides the ability to record the coordinates of points selected by the user manually. Consequently, measurement of SEM images may also be automated to some degree.

7.2 The underlying physics and chemistry

It will be clear from the emerging picture portrayed in Chapter 6 that there has been a great deal on insight gained in the last few years and, indeed, some models are beginning to emerge based on the assumed structure [62]. However, much is still very speculative. The use of Electron Paramagnetic Resonance (EPR) under the auspices of EPRI [73,74] has recently permitted the identification of oxygen radicals formed in the interface region on the introduction of nanoparticles which provides both an important springboard for the selection of appropriate particle chemical functionalization and also a means to quantify the interfacial processes. It also provides some reason to believe the mechanism suggested by Lewis [75] that the interface actually constitutes a diffuse charged region which could give rise to some local conductivity which leads to some of the properties documented. The EPR technique has also permitted, perhaps for the first time, the visualization of the formation of surface trap states through the ability to energize a dielectric sample while in the EPR spectrometer [74].

This kind of diagnostic test is currently being supplemented, as described in Chapter 5 by a number of other techniques aimed at obtaining information on the underlying processes taking place. Advanced methods such as electroluminescence and pulsed electroacoustic analysis allow differences produced through particle size, loading and surface chemistry to be used to gain the much needed insight into the operation of the internal interfaces. As the work moves forward, the preliminary work described in Section 5 will be more comprehensively studied with a particular emphasis on trying to ascertain the spatial extent of the interaction zone.

A
REFERENCES

[1]   J.K. Nelson. and J.C. Fothergill, "Internal charge behaviour in nanocomposites", Nanotechnology, Vol. 15, 2004, pp 586-9

[2]   L.A. Dissado, J.C Fothergill, "Dielectrics and nanotechnology", IEEE Transactions on Dielectrics and Electrical Insulation, Vol. 11, 2004, pp 737 – 738

[3]   M. Roy, J.K. Nelson and L. Schadler, "An examination of the potential for nano-composites in the formulation of HV cable insulation", Technical Report # 1010498, EPRI, Palo Alto, CA, Nov 2005

[4]   J.K. Nelson, L. Schadler and R.C. Smith, "The application of nanocomposite dielectrics for utility cable applications", Technical Report # 1012337, EPRI, Palo Alto, CA, Dec 2006

[5]   J.K. Nelson, L. Schadler and R. Smith, "The application of nanocomposite dielectrics for utility cable applications – Phase 2", Technical Report # 1015539, EPRI, Palo Alto, CA, November, 2007

[6]   A. Bradwell, "Electrical Insulation", Peter Peregrinus, 1983

[7]   D. Kim, J. S. Lee, C.M.F. Barry and J. Mead, "Microscopic measurement of the degree of mixing for nanoparticles in polymer nanocomposites by TEM Images", Microscopy research and technique. Vol. 70, 2007, pp 539-546

[8]   J.K. Nelson and Y. Hu, "Nanocomposite dielectrics – properties and implications", J. Phys. D: Appl. Phys, Vol. 38, 2005, pp 213-222

[9]   J.-L. Chermant and M. Coster, "Composites, microstructure of: quantitative description", Encyclopedia of materials: science and technology, pp1396-1402

[10]   M. Li, S. Ghosh, O. Richmond, H. Weiland and T.N. Rouns, "Three dimensional characterization and modeling of particle reinforced metal matrix composites: part I Quantitative description of microstructural morphology", Materials science and engineering, Vol. A265, 1999, pp153-173

[11]   P. Louis and A.M. Gokhale, "Computer simulation of spatial arrangement and connectivity of particles in three-dimensional microstructure: application to model electrical conductivity of polymer matrix composite", Acta material, Vol. 44, 1996, pp1519-1528

REFERENCES

[12]   G. Ayala, I. Epifanio, A. Simo and V. Zapater, "Clustering of spatial point patterns", Computational statistics & data analysis, Vol. 50, 2006, pp 1016-1032

[13]   A. Escudero, J.M Iriondo. and M.E Torres. "Spatial analysis of genetic diversity as a tool for plant conservation", Biological Conservation, Vol. 113, 2003, pp 351-365

[14]   W.M. Khaemba, "Spatial point pattern analysis of aerial survey data to assess clustering in wildlife distributions", International journal of applied earth observation and geoinformation, Volume 3, 2001, pp 139-145

[15]   D. Prodanoy, N. Nagelkerke and E. Marani, "Spatial clustering analysis in neuroanatomy: Applications of different approaches to motor nerve fiber distribution", Journal of neuroscience methods, Vol. 160, 2007, pp 93-108

[16]   Y. Lu and X. Chen, "On the false alarm of planar *K*-function when analyzing urban crime distributed along streets", Social science research, Vol. 36, 2007, pp 611-632

[17]   N.A.C. Cressie, "Statistics for spatial data", John Wiley & Sons, 1991

[18]   "Spatial Distribution", www.css.cornell.edu/courses/620/lecture8.ppt

[19]   K.J. Kurzydlowski and B. Ralph, "The quantitative description of the microstructure of materials", CRC Press, 1995

[20]   L. Kristensen, J. Olsen, J. Weiner, H.W Griepentrog and M. Norremark, "Describing the spatial pattern of crop plants with special reference to crop-weed competition studies", Field crops research, Vol. 96, 2006, pp 207-215

[21]   R. Kerry. and M.A. Oliver, "Determining the effect of asymmetric data on the variogram", Computers & geosciences, Vol. 33, 2007, pp 1212-1232

[22]   D. Kim, J.S. Lee, C.M.F. Barry and J.L. Mead, "Effect of fill factor and validation of characterizing the degree of mixing in polymer nanocomposites", Polymer engineering & science, Vol. 47, 2007, pp 2049-2056

[23]   A. Tewari and A.M. Gokhale, "Nearest neighbor distances in uniform–random poly-dispersed microstructures ", Materials science and engineering, Vol. A396, 2005, pp22–27

[24]   J.W. Leggoe, "Nth-nearest neighbor statistics for analysis of particle distribution data derived from micrographs", Scripta materialia, Vol. 53, 2005, pp 1263-1268

[26]   M. Ieda, T. Mizutani, and Y. Suzuoki,; *Memoirs of the Faculty of Engineering*, Nagoya University, Vol. 32, No. 2 1980

[27] S. Maeta and K. Sakaguchi, "A New Method for Determining the Trap Depth from Thermally Stimulated Current," Japanese Journal for Applied Physics, Vol.19, No.4, 1980, pp. 597-606.

[28]   R. C. Smith, C. Liang, M. Landry, J. K Nelson and. L. S Schadler, "The Mechanisms Leading to the Useful Electrical Properties of Polymer Nanodielectrics", IEEE Transactions on Dielectrics and Electrical Insulation, Vol. 15, 2008, (accepted for publication)

[29]   G. G. Raju, "Dielectrics in electric fields", Marcel Dekker, 2003

[30]   A.K. Jonscher, "Dielectric relaxation in solids," J. Phys. D: Appl. Phys. Vol 32, 1999, p R63

[31]   M. Roy, J.K. Nelson, R.K. MacCrone and L.S. Schadler, "Candidate Mechanisms Controlling the Electrical Characteristics of Silica/XLPE Nanodielectrics", J. Materials Sci., Vol. 42, 2007, pp. 3789-3799

[32]   M. Roy, J. K. Nelson, C. W. Reed, R. K. MacCrone, R. J. Keefe, W. Zenger and L. S. Schadler, "Polymer Nanocomposite Dielectrics - The Role of the Interface", IEEE Trans. Dielectr. Electr. Insul., Vol. 12, 2005, pp. 629-642,

[33]   M. F. Frechette, C.W. Reed, and H. Sedding, "Progress, understanding and challenges in the field of nanodielectrics", IEEJ Trans. Fundamentals and Materials, Vol. 126, 2006, pp. 1031-1043,

[34]   M.F. Frechette, M.L. Trudeau, H.D. Alamdari, and S. Boily, "Introductory remarks on nanodielectrics", IEEE Trans. Dielectr. Electr. Insul., Vol. 11, 2004, pp. 808-818.

[35]   T. Tanaka, "Dielectric nanocomposites with insulating properties", IEEE Trans. Dielectr. Electr. Insul., Vol. 12, 2005, pp. 914-928.

[36]   T. Tanaka, A. Matsunawa, Y. Ohki, M. Kozako, M. Kohtoh, and S. Okabe, "Treeing phenomena in epoxy/alumina nanocomposite and interpretation by a multi-core model", IEEJ Trans. Fundamentals and Materials, Vol. 126, 2006, pp. 1128-1135.

[37]   T. Imai, F. Sawa, T. Ozaki, T. Shimizu, R. Kido, M. Kozako, and T. Tanaka, "Influence of temperature on mechanical and insulation properties of epoxy-layered silicate nanocomposite", IEEE Trans. Dielectr. Electr. Insul., Vol. 13, 2006, pp. 445-452.

[38]   T. Kikuma, N. Fuse, T. Tanaka, Y. Murata, and Y. Ohki, "Filler-content dependence of dielectric properties of low-density polyethylene/MgO nanocomposites", IEEJ Trans. Fundamentals and Materials, Vol. 126, 2006, pp. 1072-1077.

[39]   J. Taima, K.I., T. Maezawa, Y. Tanaka, T. Takada and Y. Murata, "Observation of Space Charge Formation in LDPE/MgO Nano-composite under DC Stress at High Temperature", IEEE Conf. Electr. Insul. Dielectr. Phenomenon, 2006, pp. 302-305.

[40]   F. Gustavino, E.T., M. Hoyos, N. Garcia, H. Reinecke, E. Benito and P. Tiemblo, "AC Electrical Strength Measurements on LDPE Nanocomposites", IEEE Conf. Electr. Insul. Dielectr. Phenomenon, 2006, pp. 329-332.

REFERENCES

[41] J.K. Nelson, and J.C. Fothergill, "Internal charge behaviour of nanocomposites", Nanotechnology, Vol. 15, 2004, pp. 586-595.

[42] P. Murugaraj, D. Mainwaring, and N. Mora-Huertas, "Dielectric enhancement in polymer-nanoparticle composites through interphase polarizability", J. Appl. Phys., Vol. 98, 2005, p. 054304.

[43] M. Roy, *An Examination of the Potential for Nano-Composites in the Formulation of HV Cable Insulation*, Ph.D. dissertation, Dept. of Electrical, Computer, and Systems Engineering, Rensselaer Polytechnic Institute, 2005.

[44] R.J. Fleming, A. Ammala, P.S. Casey, and S.B. Lang, "Electrical conductivity in LDPE containing nano- and micro-sized ZnO particles", IEEE Conf. Electr. Insul. Dielectr. Phenomenon, 2007, pp. 25-28.

[45] R. Kurnianto, "Electrical treeing breakdown in inorganic-filler/LDPE nano-composite material", IEEJ Trans. Fundamentals and Materials, Vol. 127, 2007, pp. 29-34.

[46] H.T. Vo and F.G. Shi, "Towards model-based engineering of optoelectronic packaging materials: Dielectric constant modeling", Microelectronics J., Vol. 33, 2002, pp. 409-415.

[47] J.K. Nelson and Y. Hu, "Nanocomposite dielectrics - Properties and implications", J. Phys. D: Appl. Phys., Vol. 38, 2005, pp. 213-222.

[48] C. Zilg, D. Kaempfer, R. Thomann, R. Muelhaupt, and G.C. Montanari, "Electrical Properties of Polymer Nanocomposites Based upon Organophilic Layered Silicates", IEEE Conf. Electr. Insul. Dielectr. Phenomenon, 2003, pp. 546-550.

[49] Y. Hu, R. C. Smith, J. K. Nelson and L.S. Schadler, "Some mechanistic understanding of the impulse strength of nanocomposites", IEEE Conf. Electr. Insul. Dielectr. Phenomenon, 2006, pp. 31-34.

[50] R. Sarathil, R. K. Sahu, P. R. Kumar, and T. Tanaka, "Understanding the Performance of Epoxy Nano Composites - A Physico-Chemical Approach", IEEJ Trans. Fundamentals and Materials Vol. 126, 2006, pp. 1112-1120.

[51] J. K. Nelson and Y. Hu, "The impact of nanocomposite formulations on electrical voltage endurance", IEEE 8th Int. Conf. on Solid Dielectrics, 2004, pp. 68-73.

[52] N. Fuse, M. Kozako, T. Tanaka, S. Murase, and Y. Ohki, "Possible Mechanism of Superior Partial-Discharge Resistance of Polyamide Nanocomposites", IEEE Conf. Electr. Insul. Dielectr. Phenomenon, 2004, pp. 322-325.

[53] J. K. Nelson and Y. Hu, "Candidate Mechanisms Responsible for Property Changes in Dielectric Nanocomposites", IEEE Int. Conf. on Properties and Applications of Dielectric Materials, 2006, pp. 150-153.

A-4

[54] Y. Yin, J. Chen, J. Yang, D. Xiao, D. Tu, R. Yin, and H. Qian, "Effect of Space Charge in Nanocomposite of LDPE/TiO2", IEEE Int. Conf. on Properties and Applications of Dielectric Materials, 2003, p. 913916.

[55]   T.J. Lewis, "Interfaces and nanodielectrics are synonymous", Proc. IEEE Int. Conf. on Solid Dielectrics, Toulouse, France, Vol.2, 2004, pp. 792-795.

[56] Z. Xiao, Y. Li, D. Ma, L. S. Schadler, and Y.A. Akpalu, "Probing the use of small-angle light scattering for characterizing structure of titanium dioxide/low-density polyethylene nanocomposites", J. Polymer Sci., Part B: Polymer Phys., Vol. 44, 2006, pp. 1084-1095.

[57]   H. Yang, P. Bhimaraj, L. Yang, R.W. Siegel, and L.S. Schadler, "Crystal Growth in Alumina/Poly(ethylene terephthalate) Nanocomposite Films", J. Polymer Sci., Part B: Polymer Phys., Vol.45, Iss.7, 2006, pp. 747-757.

[58] T. Desai, P. Keblinski, and S.K. Kumar, "Molecular dynamics simulations of polymer transport in nanocomposites", J. Chem. Phys., Vol. 122, 2005, p. 134910.

[59] K.S. Gautam and A. Dhinojwala, "Molecular structure of hydrophobic alkyl side chains at comb polymer-air interface", Macromolecules, Vol. 34, 2001, pp. 1137-1139.

[60] A.J. Zhu and S.S. Sternstein, "Reinforcement mechanism of nanofilled polymer melts as elucidated by nonlinear viscoelastic behavior", Macromolecules, Vol. 35, pp. 7262-7273, 2002.

[61] K.E. Atkinson and C. Jones, "Study of the interphase region in carbon fibre/epoxy composites using dynamic mechanical thermal analysis", J. Adhesion, Vol. 56, 1996, pp. 247-260.

[62] T. Tanaka, M. Kozako, N. Fuse, and Y. Ohki, "Proposal of a multi-core model for polymer nanocomposite dielectrics", IEEE Trans. Dielectr. Electr. Insul., Vol. 12, 2005, pp. 669-681.

[63]   T. J. Lewis, "Interfaces: Nanometric dielectrics", J. Phys. D: Appl. Phys., Vol. 38, 2005, pp. 202-212.

[64] B.J. Ash, R.W. Siegel and L.S. Schadler, "Glass-Transition Temperature Behavior of Alumina/PMMA Nanocomposites," J. Polymer Sci. Part B, Polymer Phys., Vol. 42, 2004, pp. 4371-4383.

[65] C. Becker, H. Krug, and H. Schmidt, "Tailoring of thermomechanical properties of thermoplastic nanocomposites by surface modification of nanoscale silica particles," Mater. Res. Soc. Symp. Proc., 435, 1996, pp. 237-242.

[66] Y. Kojima, A. Usuki, M. Kawasumi, A. Okada, T. Kurauchi, O. Kamigaito and K. Kaji, "Fine-structure of nylon-6-clay hybrid," J. Polym. Sci.: Part B: Polymer Phys., Vol. 32 (4), 1994m pp. 625-630.

REFERENCES

[67] Z. Xiao, Y. Li, D. Ma, L. S. Schadler, and Y. A. Akpalu, "Probing the use of Small-Angle Light Scattering for Characterizing Structure of Titanium Dioxide/Low Density Polyethylene Nanocomposites", J. Polymer Sci. Part B: Polymer Phys., Vol. 44, 2006, pp. 1084-1095.

[68] S. Sternstein and A. Zhu, "Reinforcement mechanism of nanofilled polymer melts as elucidated by nonlinear viscoelastic behavior", Macromolecules, Vol. 35, 2002, pp. 7262-7273.

[69] R.C. Smith, C. Liang, M. Landry, J.K. Nelson, and L.S. Schadler, "Studies to unravel some underlying mechanisms in nanodielectrics," IEEE Conf. Electr. Insul. Dielectr. Phenomena, 2007, pp. 286-289.

[70] A. Many and G. Rakavy, "Theory of Transient Space-Charge-Limited Currents in Solids in the Presence of Trapping", Phys. Rev., Vol. 126, 1962, pp. 1980-1988.

[71] R. Vogelsang, R. Brutsch, and K. Frohlich, "Effect of electrical tree propagation on breakdown in mica insulations", 13th Int. Symp. H.V. Engineering, 2003, pp. 375-378.

[72] N. Fuse, M. Kozako, T. Tanaka, S. Murase, and Y. Ohki, "Possible Mechanism of Superior Partial-Discharge Resistance of Polyamide Nanocomposites", IEEE Conf. Electr. Insul. Dielectr. Phenomenon, 2004, pp. 322-325.

[73] J.K. Nelson, R.K. MacCrone, L.S. Schadler, R. Smith and R.J. Keefe," The use of Electron Paramagnetic Resonance in the probing of the nanodielectric interface", IEEE Int. Conf. on Solid Dielectrics, Winchester, UK, 2007, pp 428-31

[74] J.K. Nelson and R.K. MacCrone, "Tools for engineering nanodielectrics", Technical Report # 1015537, EPRI, Palo Alto, CA, November 2007

[75] T.J. Lewis, "Interfaces are the dominant feature of dielectrics at the nanometric level", IEEE Trans EI. Vol. 11, 2004, pp 739-53.

Export Control Restrictions

Access to and use of EPRI Intellectual Property is granted with the specific understanding and requirement that responsibility for ensuring full compliance with all applicable U.S. and foreign export laws and regulations is being undertaken by you and your company. This includes an obligation to ensure that any individual receiving access hereunder who is not a U.S. citizen or permanent U.S. resident is permitted access under applicable U.S. and foreign export laws and regulations. In the event you are uncertain whether you or your company may lawfully obtain access to this EPRI Intellectual Property, you acknowledge that it is your obligation to consult with your company's legal counsel to determine whether this access is lawful. Although EPRI may make available on a case-by-case basis an informal assessment of the applicable U.S. export classification for specific EPRI Intellectual Property, you and your company acknowledge that this assessment is solely for informational purposes and not for reliance purposes. You and your company acknowledge that it is still the obligation of you and your company to make your own assessment of the applicable U.S. export classification and ensure compliance accordingly. You and your company understand and acknowledge your obligations to make a prompt report to EPRI and the appropriate authorities regarding any access to or use of EPRI Intellectual Property hereunder that may be in violation of applicable U.S. or foreign export laws or regulations.

The Electric Power Research Institute (EPRI)

The Electric Power Research Institute (EPRI), with major locations in Palo Alto, California; Charlotte, North Carolina; and Knoxville, Tennessee, was established in 1973 as an independent, nonprofit center for public interest energy and environmental research. EPRI brings together members, participants, the Institute's scientists and engineers, and other leading experts to work collaboratively on solutions to the challenges of electric power. These solutions span nearly every area of electricity generation, delivery, and use, including health, safety, and environment. EPRI's members represent over 90% of the electricity generated in the United States. International participation represents nearly 15% of EPRI's total research, development, and demonstration program.

Together…Shaping the Future of Electricity

1013885